XRCC4 deficiency in human subjects causes a marked neurological phenotype but no overt immunodeficiency

Article (Accepted Version)

XRCC4-deficiency in humans causes a marked neurological phenotype but no overt immunodeficiency

Chaowan Guo[1,2,3,11], Yuka Nakazawa[1,2,3,11], Lisa Woodbine[4,11], Andrea Björkman[5], Mayuko Shimada[2,3], Heather Fawcett[4], Nan Jia[1,2,3], Kaname Ohyama[2,6], Taosheng Li[7], Yuji Nagayama[3], Norisato Mitsutake[2,8], Qiang Pan-Hammarström[5], Andrew R Gennery[9], Alan R Lehmann[4], Penny A Jeggo[4,*], Tomoo Ogi[1,2,3,10,*]

[1]Department of Genetics, Research Institute of Environmental Medicine (RIeM), Nagoya University, Furo-cho, Chikusa-ku, Nagoya, 464-8601, Japan; [2]Nagasaki University Research Centre for Genomic Instability and Carcinogenesis (NRGIC), 1-12-4, Sakamoto, Nagasaki, 852-8523 Japan; [3]Department of Molecular Medicine, Atomic Bomb Disease Institute, Nagasaki University, 1-12-4 Sakamoto, Nagasaki, 852-8523, Japan; [4]Genome Damage and Stability Centre, University of Sussex, Falmer, Brighton, BN1 9RQ, United Kingdom; [5]Department of Laboratory Medicine, Karolinska Institutet, Karolinska University Hospital, Huddinge, SE-14186 Stockholm, Sweden; [6]Course of Pharmaceutical Sciences, Graduate School of Biomedical Sciences, Nagasaki University, 1-14, Bunkyo, Nagasaki 852-8521 Japan. [7]Department of Stem Cell Biology, Atomic Bomb Disease Institute, Nagasaki University, 1-12-4, Sakamoto, Nagasaki, 852-8523 Japan; [8]Department of Radiation Medical Sciences, Atomic Bomb Disease Institute, Nagasaki University, 1-12-4 Sakamoto, Nagasaki, 852-8523, Japan; [9]Institute of Cellular Medicine, Newcastle University, Newcastle upon Tyne Hospitals NHS Foundation Trust, Newcastle upon Tyne, United Kingdom; [10]Microbial Genetics Laboratory, Genetic

24 Strains Research Center, National Institute of Genetics, 1111 Yata, Mishima 411-8540,
25 Japan; [11]These authors contributed equally to this work.
26
27 *Correspondence: togi@riem.nagoya-u.ac.jp (T.O), p.a.jeggo@sussex.ac.uk (P.A.J.)
28

Abstract

Background: Non-homologous end-joining (NHEJ) is the major DNA double strand break (DSB) repair mechanism in human cells. The final rejoining step requires DNA ligase IV (LIG4), together with partner proteins, XRCC4 and XLF. Patients mutated in genes encoding LIG4, XLF or other NHEJ proteins DNA-PKcs and Artemis are DSB repair defective and immunodeficient, due to the requirement for NHEJ during V(D)J recombination.

Objective: We found a patient displaying microcephaly and progressive ataxia but a normal immune response. We sought to determine pathogenic mutations and to describe a molecular pathogenesis of the patient.

Methods: We performed NGS exome sequencing. We evaluated DSB repair activities and V(D)J recombination capacity of the patient cells as well as a standard blood immunological characterisation.

Results: We identified causal mutations in the *XRCC4* gene. The patient cells are radiosensitive and display the most severe DSB repair defect that we have encountered using patient derived cell lines. In marked contrast, a V(D)J recombination plasmid assay revealed that the patient cells did not display the junction abnormalities that are characteristic of other NHEJ-defective cell lines. The mutant protein can interact efficiently with LIG4 and functions normally in *in vitro* assays and when transiently expressed *in vivo*. However, the mutation makes the protein unstable and it undergoes proteasome-mediated degradation.

Conclusion: Our findings reveal a novel separation of impact phenotype: there is a

pronounced DSB repair defect and marked clinical neurological manifestation but no clinical immunodeficiency.

Capsule Summary

A patient with mutations in the *XRCC4* gene, encoding a DNA double-strand-break (DSB) repair factor, displayed severe radiosensitivity and neurological abnormalities but maintained normal V(D)J recombination function. Our findings suggest a separation of impact phenotype.

Key Words

DNA double strand break (DSB) repair; non-homologous end joining (NHEJ); DSB repair-deficiency; XRCC4/LIG4; immunodeficiency; microcephaly

Abbreviations

NHEJ: Non-homologous end-joining
CSR: Class switch recombination
CID/SCID: Combined or severe combined immunodeficiency
DSB: DNA double strand break
hTERT: Human telomerase reverse transcriptase
RRS: Recovery of RNA synthesis
UDS: Unscheduled DNA synthesis
RDS: Recovery of DNA synthesis
NMD: Nonsense mediated mRNA decay
PARP: poly ADP ribose polymerase
NER: Nucleotide excision repair

Introduction

DSBs arise from oxidative damage and during processes such as meiosis or V(D)J recombination. They are also the major lethal lesions generated in cellular DNA by ionizing radiation. Although DSBs do not arise at high frequency endogenously, they are a critical lesion causing cell death or carcinogenesis if misrepaired. Additionally, the development of the immune response involves the introduction of DSBs to generate the requisite genetic diversity.[1] V(D)J recombination represents one such process.[2] Class switch recombination (CSR), which involves the switching of immunoglobulin isotypes, also involves the introduction and rejoining of DSBs.[3]

NHEJ is the major DSB repair process in mammalian cells. The process is initiated by the binding of the Ku heterodimer to double-stranded DNA ends followed by the recruitment of the DNA-dependent protein kinase catalytic subunit, DNA-PKcs, generating the DNA-PK holoenzyme and activating DNA-PK activity.[4] DNA-PK has a role in end-tethering and regulates steps of end-processing. The final step of rejoining involves the recruitment of a ligation complex encompassing DNA ligase IV (LIG4), XRCC4 and XLF. LIG4 and XRCC4 interacts strongly via a tandem BRCT domain in LIG4 and a coiled coil region in XRCC4, forming a highly stable complex.[5, 6] XRCC4 is required for LIG4 stabilisation but recent findings have shown an excess of XRCC4 relative to LIG4.[7] Mutations that abolish LIG4/XRCC4 interaction prevent all NHEJ activity. XLF is a weaker binding partner. XRCC4 and XLF are structurally similar; both have a globular head domain, but the coiled coil region of XLF is shorter than that in XRCC4.[8, 9] Recent studies have reported that dimers of XRCC4 and XLF interact to form long superhelical filaments in solution, which have been proposed to promote

end-tethering or end-bridging downstream of the DNA-PK complex.[8, 10-12]

Loss of LIG4 or XRCC4 confers embryonic lethality in mice due to extensive neuronal apoptosis.[13, 14] In contrast, XLF null mice are viable and do not show marked immunodeficiency.[15] Mutations in *LIG4*, *DCLRE1C* (Artemis), *NHEJ1* (XLF) and *PRKDC* (DNA-PKcs) in patients have been described.[16-20] LIG4 syndrome, which is caused by hypomorphic mutations in *LIG4*, is characterised by growth delay, microcephaly, and combined or severe combined immunodeficiency (CID/SCID). LIG4 syndrome cell lines show radiosensitivity, diminished ability to repair DSBs and impaired V(D)J recombination. XLF defective patients, some of which have null mutations, display features similar to, although often more severe than LIG4 syndrome.[18] Given the close interaction and requirement of XRCC4 for LIG4 stability, the expectation was that XRCC4 deficiency in patients would resemble LIG4 syndrome.

In contrast to this expectation, an XRCC4-deficient patient, CSL16NG, whose cellular defects we describe in this paper, displayed unique clinical features similar to those of Cockayne Syndrome, namely progressive neuronal degeneration including the onset of ataxia, but no clinical immunodeficiency. Our cellular analysis revealed that the mutational changes result in substantially reduced levels of XRCC4 protein, a marked defect in DSB repair but seemingly efficient V(D)J recombination. Based on comparative studies with LIG4 and XLF deficient cell lines, our results reveal a separation of impact phenotype where marked deficiency in radiation-induced DSB repair capacity can be uncoupled from defective V(D)J recombination. Our results give novel insights into the roles of XRCC4 during DSB repair.

Methods

Human studies

Patient and control samples were obtained with local ethical approvals [University of Sussex Research Ethics Committee; Nagasaki University Ethical, Legal and Social Implications (ELSI) committee; Ethics committee for human genome studies in Research Institute of Environmental Medicine, Nagoya University]. Written informed consent was obtained from the patient.

Exome sequencing and bioinformatics

Details are described in **Supplementary Methods**. Briefly, genomic DNA prepared from CSL16NG fibroblasts was enriched using the SureSelect All Exon Kit v5 (Agilent), followed by sequencing on the Illumina Hiseq 2500 sequencer. The sequence data were analysed by a standard exome pipeline. According to a recessive inheritance model, we selected genes that carried at least one novel deleterious homozygous or more than two heterozygous changes in one gene locus (**Table S1**).

Cell cultures

Human primary or hTERT immortalized fibroblasts were derived from the XRCC4 patient (CSL16NG), LIG4 patients (F07/614, 180BR, 411BR, 2303 and 495GOS), *XLF* patients (2BN and F07/402), an XP patient (XP15BR) or healthy donors (1BR.3 and 48BR). All primary fibroblasts were cultured in Dulbecco′s Modified Eagle Medium (DMEM) or Modified Eagle Medium (MEM), supplemented with 10-15 % fetal bovine serum (FBS) and 1× penicillin-streptomycin (PS). HEK293FT cells (Invitrogen) were grown in DMEM supplemented with 10 % FBS, 1× PS, 5 mM L-glutamine, 0.1 mM

147 Non-Essential Amino Acids (NEAA) and 1 mM sodium pyruvate. Human colon cancer
148 HCT116 (RCB2979) and HCT116-XRCC4 (-/-) (RCB2981) cells were provided by the
149 RIKEN BRC through the National Bio-Resource Project of the MEXT, Japan.
150
151 **Reagents and Antibodies**
152 Antibodies used were: XRCC4 (C4 and C20, Santa Cruz Biotechnology), LIG4 (D8,
153 Santa Cruz Biotechnology; Ab80514, Abcam; 12695-1-AP, Proteintech Group), p89
154 (S-19, Santa Cruz Biotechnology), XPG (8H7, Santa Cruz Biotechnology), CSB (Bio
155 Matrix Research), V5-tag (MBL), Flag-tag (MBL), Actin (Ab8227, Abcam),
156 Alpha-tubulin (Invitrogen), XLF (ab33499, Abcam; FL-299, Santa Cruz Biotechnology),
157 53BP1 (Bethyl) and gamma H2A.X (ser139, Millipore). MG132, E64D,
158 3-Methyladenine (3-MA), Epoxomicin, and Cycloheximide (CHX) (Sigma-Aldrich).
159
160 **Quantitative RT-PCR**
161 Details are as described previously.[21] Total RNA was extracted using the RNeasy Plus
162 Mini Kit (QIAGEN). The High-capacity RNA-to-cDNA kit (Applied Biosystems) was
163 used for 1st strand synthesis. Quantitative PCR was performed using the Thermal
164 Cycler Dice Real-Time system (TaKaRa Bio) with a QuantiTect SYBR Green PCR Kit
165 (QIAGEN). For each sample, the relative mRNA expression levels were normalized
166 using the *HPRT1* gene. Error bars represent the S.D. of means of triplicate experiments.
167
168 **Lentivirus experiments**
169 Details are as described previously.[22] Recombinant lentivirus particles expressing
170 *XRCC4* and its mutants were produced. Human *XRCC4* cDNA was cloned in frame

with a C-terminal V5-tag in the *pLenti6.3*-V5-D-TOPO vector to generate *pLenti6.3-XRCC4*-V5 plasmid. The truncation mutant (XRCC4-Del), the frameshift mutant (XRCC4-Fs), and the single amino-acid substitution mutant (XRCC4-W43R) were generated from *pLenti6.3-XRCC4*-V5 by site-directed PCR mutagenesis. Sequences of the mutant plasmids were confirmed by Sanger sequencing (**Figure S1**). 48 hours after lentivirus infection, 10 μg/ml of blasticidin (Sigma-Aldrich) was added to the medium for selection of XRCC4 stably expressing cells.

Ionizing irradiation and γH2AX foci assay

Cells were seeded in 3 cm dishes or in 96-well plates (BD Falcon) and 3Gy γ-ray irradiated using a ^{137}Cs γ-ray source at a dose rate of 0.017 Gy s^{-1}, then further cultured for indicated time periods. Cells were fixed with 4 % formaldehyde and permeabilized with 0.2 % TritonX-100, followed by staining with DAPI and γH2AX antibody. Image acquisition and analysis were performed using the Cellomics ArrayScan VTI (Thermo Scientific). The average number of separate γH2AX foci was assessed on at least 300 cells.

NHEJ-, V(D)J- and CSR assays

The assays were performed as previously described.[23, 24] For NHEJ-assay, 1 μg PDVG94 plasmid, digested with *Eco*RV and *Eco*47III (Promega) to create blunt ends with 6 bp repeats, were transiently transfected into fibroblast cells using Turbofect (Fermentas). 48 h after transfection, cells were harvested and DNA extracted using DNeasy blood and tissue kit (QIAGEN). The recombined junctions were PCR amplified with primers FM30 and DAR5[23] and the PCR product was gel purified using Qiaquick

gel extraction kit (QIAGEN), cloned into pGEM-T vectors and sequenced (Macrogen). The V(D)J-assay was performed as the NHEJ-assay except that in total 1.5 μg of PDVG93 circular plasmid, RAG1 and RAG2 plasmids were transiently transfected into fibroblast cells and the coding junctions were amplified by a nested PCR using the primers NV05F (5'-CTATAGGGGAATTGTGAGCGGATAACDG-3'), DG147 and DG89, FM30.[23] Switch recombination junctions were PCR amplified, cloned, sequenced and analysed as described previously.[25, 26]

Protein purification

Detailed protein purification procedures and buffer conditions are as described previously.[21, 27] Briefly, HEK293FT cells were co-transfected with the *pLenti6.3-LIG4*-His and *pLenti6.3*-Flag-*XRCC4*, or its mutants. Cell lysates were incubated with anti-Flag M2 beads (Sigma-Aldrich) for 4 hours at 4 °C. After extensive washing of the beads, the Flag-tagged wild type (WT) or mutant XRCC4 in complex with LIG4 was eluted with Flag-peptide. The eluted complexes were dialyzed, concentrated and stored at -80°C. For expression and purification of GST-XLF protein, *E.coli* BL21 (DE3) cells were transformed with *pGEX6*-GST-*XLF* plasmid. The GST-XLF protein was induced with IPTG. The cells were harvested, lysed and cleared lysate was loaded onto a GSTrap HP column (GE Healthcare). After washing, the GST-XLF protein was eluted by reduced L-glutathione (Wako). The eluted proteins were dialyzed, concentrated and stored at -80°C.

***In vitro* DSB ligation assay**

A 934 bp Cy5-labeled double strand DNA fragment was PCR amplified from pEGFP-C3 vector using a set of primers (Forward: 5'-Cy5-GTTTCGCCACCTCTGACTTGAGCG-3'; Reverse: 5'-GAACTTCAGGGTCAGCTTGCCGTAG-3'). The DNA fragment was digested with *Nco*I (TaKaRa). A 545 bp fragment (Cy5 labeled at the 5' blunt-end and a 3'-overhang end) and a 255 bp fragment (with 4 bp overhangs at each end) were purified. The complexes were incubated for 30 min at 37 °C in a 30 μl reaction mixture (66 mM Tris-HCl pH7.5, 5 mM $MgCl_2$, 1 mM DTT, 1 mM ATP) with 50 ng of DNA substrates (the Cy5-labeled 545 bp fragment: the unlabeled 255 bp fragment = 2: 3). Reaction mixtures were pre-incubated for 10 min on ice with GST-XLF, and then LIG4-XRCC4 complex was added at 37 °C for 15 min. The reactions were terminated by adding 1.5 μl of 10 % SDS, followed by purification with QIAquick PCR Purification kit (QIAGEN). 30 μl of the eluted DNA was mixed with 10× loading buffer, incubated at 65 °C for 5 min and cooled on ice rapidly. 15 μl of the DNA was run on 1 % agarose gel and analyzed by the Typhoon imager (GE Healthcare).

Analysis of protein stability

HEK293FT cells were transiently transfected with XRCC4 or its mutant plasmids. Cells were treated with CHX (100 μg/ml) combined with MG132 (20 μM), E64D (20 μM), Epoxomicin (1 μM) or 3-MA (10 mM). Cells were harvested at the indicated time points. Whole cell lysate was analysed by Western blotting using anti-V5 antibody.

Immunoprecipitation

Immunoprecipitation of ectopically expressed WT or mutant XRCC4 proteins in

CSL16NG cells was performed on cell extracts using anti-V5 agarose (MBL). Immunoprecipitates were washed five times with lysis buffer containing 0.15 or 1 M NaCl, then eluted using V5-peptide (2 mM, MBL). The eluted proteins were separated on 5-20 % gradient SDS-PAGE gels, blotted onto PVDF membranes and analyzed by Western blotting.

Confocal Fluorescence Microscopy

Cells were washed once with PBS (Wako) and fixed with Fix buffer [300 mM sucrose, 2 % (v/v) formaldehyde, and 0.2 % (v/v) Triton X-100 in PBS]. After a brief washing in PBS, cells were blocked with 10 % FBS in PBS for 30 min and then incubated for 1 h with the anti-V5-tag, anti-γH2AX, anti-LIG4 or anti-XRCC4 antibodies at appropriate dilution. The cells were then washed three times with PBST (0.05 % Tween-20) and incubated with Alexa fluor488-conjugated secondary antibody at a dilution of 1:500 for 1 h. To visualize nuclei, the cells were incubated with DAPI (10 ng/mL) for 15 min. Cells were then washed and mounted, and examined on a LSM 700 laser scanning confocal microscope (Carl Zeiss). Images were taken with the 40× oil immersion objective lens under identical imaging settings.

Survival analysis

Fibroblasts were irradiated using a ^{137}Cs γ-ray source at a dose rate of 0.09 Gy s^{-1}. Radiosensitivity was assessed by colony survival analysis. Cells were trypsinised, irradiated and plated onto feeder cells prepared 24 h earlier and left to form colonies for three weeks. For XRCC4 complementation experiments, normal (48BR), CSL16NG and CSL16NG-derived fibroblasts expressing WT XRCC4 were seeded in 96-well

plates (BD Falcon). After γ-ray irradiation, cells are incubated for a further 24 hours. Sensitivity to IR was measured by recovery of DNA synthesis (RDS) analysis as described in supplementary methods (RRS, UDS and RDS assays).

Results

Patient CSL16NG has compound heterozygous mutations in *XRCC4*

Patient CSL16NG, the first daughter of non-consanguineous Caucasian parents, had significant intrauterine growth failure and microcephaly at birth. She showed slow growth, delayed motor development and dysmorphic features. Her stature, developmental delay, deep-set eyes and other features resembled those of Cockayne syndrome (CS). However, she had no history of photosensitivity and relatively slow progression of symptoms. She developed progressive ataxia. At 19 years, she was diagnosed with a low-grade thalamic glioma, which was not removed. She has hyperopia, diabetes mellitus, hypothyroidism, moderate hearing loss and slurred speech, although her understanding remains good. Her neurology has been described previously (Patient 3 in[28]). She has no significant infectious history and no obvious signs of abnormal immune response. Detailed routine blood immunological peripheral blood tests did not reveal any abnormality. Blood cell counts including peripheral blood lymphocyte sub-type numbers, immunoglobulin IgM, IgG and IgA levels were normal. Autoantibodies were negative and specific vaccine antigen antibody responses were present (**Table S2**). She is currently 23 years old (Her weight is 41.4 kg (<<3rd centile), head circumference 42.5 cm (<<3rd centile) (**Figure 1A**).

As a diagnosis of CS was considered, cellular tests for abnormal responses to UV light were carried out on a fibroblast culture established from a skin biopsy, but no abnormality typical of CS cells was observed (**Figures S2A-C**). Heterozygous mutations in two CS-related genes (*ERCC6/CSB* and *ERCC5/XPG*) were identified but both alleles were inherited from the asymptomatic father. Both proteins were expressed at normal levels (**Figures S2D and S2E**). Whole exome sequencing was carried out and

of the five potentially pathogenic candidate genes identified (details are described in **Supplemental Method; Tables S1**) *XRCC4* was the strongest. One mutation (c.C673T, p.R225*) introduced a premature stop codon; the second mutation (c.G760del, p.D254fs*68) was a frameshift (**Figure S3A**, confirmed by Sanger gDNA sequencing), which predicted the expression of a protein with an aberrant C-terminal 68 amino acids (aa), resulting in a 322 aa protein (normal full-length protein has 334 aa).

Allele-specific quantitative RT-PCR (qRT-PCR) using primers that selectively amplify the wild type (WT) or the mutant *XRCC4* cDNAs (**Figure S3B** and in **Table S3**) revealed extremely low expression of the p.R225* allele, consistent with strong nonsense mediated mRNA decay (NMD) caused by the premature stop codon (**Figure S3C**, middle panel; **Figure S3D**, left panel). The other allele encompassing the p.D254fs*68 frameshift mutation (designated as XRCC4-Fs hereafter) was expressed at ~30% of the total *XRCC4* expression level in normal 48BR cells (50% would be expected if fully expressed from one allele). The small decrease in the frameshift transcript level could reflect some NMD, although we note that the newly generated premature termination codon is located in the last exon, which does not normally trigger NMD. The mutational change could additionally affect the splicing efficiency or accuracy, which may also cause NMD (**Figure S3D**, middle panel; **Figure S3C**, left panel). No detectable XRCC4 was observed by immunoblotting of CSL16NG cells using a mouse anti-XRCC4 antibody with an epitope located close to the N-terminus of XRCC4 (**Figure 1B**). We could detect XRCC4 from a control fibroblast diluted ten-fold arguing that there is less than 10% of the normal level of XRCC4 in the patient cells.

XRCC4 is reported to co-stabilise LIG4.[5, 29, 30] Consistently, LIG4 was significantly reduced in CSL16NG fibroblasts assessed by immunoblotting (**Figure 1B,**

318 **1C**). The level of LIG4 appeared to vary depending on conditions and antibody (see
319 **Figure 1B**, 2nd and 3rd panel). When compared with the *LIG4*-null cell line N114P2
320 (LIG4-/-), a band of LIG4 was clearly visible (**Figure 1C**) and, from the results of many
321 experiments, we estimate a residual level of between 5 and 15% of normal. We also
322 analysed XRCC4 expression by immunofluorescence (IF), which revealed a low signal
323 in CSL16NG cells detectable in both the cytoplasm and nucleus (**Figure 1D**).
324
325 **CSL16NG cells are radiosensitive and DSB repair defective.**
326 CSL16NG primary fibroblasts showed marked radiosensitivity relative to control cells
327 (**Figure 2A and Figure S4**) and reduced recovery of replication after radiation exposure
328 **(Figure 2B)**. Further, CSL16NG cells showed diminished DSB repair capacity, assessed
329 by enumerating γH2AX foci (**Figure 2C**, compare red and white bars). In order to
330 confirm that these defects are attributable to the mutation in XRCC4, we analysed the
331 ability of WT XRCC4 to correct the defect in CSL16NG cells. When lentivirus
332 expressing *XRCC4*-Wt cDNA was used to infect CS16LNG cells, both the ability to
333 synthesise DNA after irradiation (**Figure 2B**) and the repair of DSBs (**Figure 2C**, green
334 bars) were restored to normal levels.
335
336 **CSL16NG cells are defective in a plasmid DSB rejoining assay**
337 We next examined the fidelity of repair in CSL16NG cells using an NHEJ end-joining
338 assay that involved transfection of CSL16NG cells and control cells with linearised
339 blunt end plasmids encompassing a 6 bp identical repeat at both DNA ends.[23] Whereas
340 the junctions from control cells were preferentially repaired by direct end-joining, this
341 type of repair was nearly absent in CSL16NG cells (2 % vs 72 % in control, **Table 1**).

342 Instead, the repair of CSL16NG cells was mediated by the usage of 6 bp
343 microhomology (78 % vs 8 % in controls) at the junctions, consistent with the loss of
344 efficient NHEJ in CSL16NG cells. A similar skewed repair pattern has previously been
345 observed in XLF-deficient cells.[24] These findings demonstrate a marked impact of the
346 mutation on the fidelity of DSB repair.
347
348 **CSL16NG cells carry out V(D)J recombination with enhanced fidelity compared to**
349 **control cells**
350 Defects in NHEJ are usually associated with immunodeficiency. Surprisingly,
351 CSL16NG has no history of chronic infections, and clinical analysis verified a normal
352 immune response (see above). To assess the capacity of CSL16NG cells to carry out
353 V(D)J recombination, we co-transfected CSL16NG cells with RAG1/2 expressing
354 plasmids together with a V(D)J substrate and assessed the fidelity of recombination.[23]
355 Strikingly, in contrast to the NHEJ assay, most coding junctions were accurately
356 rejoined with little use of microhomology or deletion formation (**Table 2**). This novel
357 V(D)J recombination phenotype contrasts with the pattern obtained with cell lines
358 derived from most LIG4 syndrome and XLF-deficient patients, where coding junctions
359 are characterized by increased deletions and microhomology usage.[16, 18, 23, 31]
360
361 **CSL16NG cells show altered repair pattern during class switch recombination**
362 To assess class switch recombination (CSR), we examined peripheral blood
363 mononuclear cells (PBMC) from CSL16NG. The patient was aged 22 when tested, thus
364 we compared her CSR junctions to our previously published 154 Sμ-Sα junctions from
365 healthy adults (**Table 3, Figure S5**). Amplification of Sμ-Sα junctions from *in vivo*

switched B lymphocytes from the patient revealed a reduced frequency of junctions repaired by direct end-joining, albeit not to a significant degree (5% vs. 18% in controls, χ^2, p=0.15), and a markedly increased frequency of repair by unusually long microhomologies (≥10 bp; 36% vs. 3% in controls). The altered pattern was similar to, but less prominent than that previously observed in XLF and LIG4 deficient patients.[24, 32] Thus, although the patient has a normal level of serum IgA, the altered pattern of the CSR junctions still clearly suggests a defect in the recombination process, which relies on the classical NHEJ machinery.

Effect of XRCC4-Fs mutation on XRCC4 function

We next examined the impact of XRCC4-Fs on XRCC4 function and protein expression. We also examined two other forms of XRCC4 protein (**Figure S6A**): XRCC4-Del has a stop codon at the position of the frameshift mutation in CSL16NG, and thus lacks the C-terminal aberrant polypeptide. XRCC4-W43R, contains an amino acid substitution p.W43R previously identified in a primordial dwarfism (PD) patient.[33] Although Trp43 is conserved, there is no current evidence for causality. Following lentivirus infection as described above, we found that all forms of the protein were expressed (**Figure S6B**). Strikingly, normal DSB-repair activity was restored, not only by expression of WT XRCC4, but also by XRCC4-Fs. Further, XRCC4-Del also complemented the CSL16NG DSB repair defect whereas XRCC4-W43R showed little complementation (**Figure 2C**, purple, blue and orange bars). Lentiviral expression results in *XRCC4* overexpression. To examine DSB repair under physiological expression levels, we also used hTERT-immortalised CSL16NG cells in a plasmid based complementation assay (**Figure S7**) and measured DSBs as 53BP1 foci in cells containing the plasmid. Full

complementation was found using WT XRCC4 protein and substantial, although not full, correction by XRCC4-Fs (**Figure S7B**). Untransfected cells in the same population showed the expected DSB repair defect.

These findings suggest that the mutant protein can partially function in DSB repair. This function likely contributes to the residual DSB repair capacity observed in CSL16NG cells. We also conclude that the W43R mutation impairs XRCC4 function.

Biochemical characterisation of the mutant XRCC4 proteins

To further examine the functional capacity of XRCC4-Fs, we purified recombinant XRCC4-LIG4 complexes and examined their activity *in vitro*. Flag-tagged XRCC4-Wt, XRCC4-Fs, and XRCC4-Del proteins were co-expressed with WT His-tagged LIG4 in HEK293FT cells and co-purified by affinity chromatography (**Figure 3A**; GST-XLF was purified from *E.coli* in **Figure 3B**). XRCC4-Fs and XRCC4-Del formed complexes with LIG4, demonstrating that the XRCC4 C-terminus is dispensable for complex formation.

In vitro ligation assays were performed using a fluorescent-labeled double strand DNA with a 3' overhang on one side and an additional smaller double strand DNA substrate with the same 3' cohesive overhang on both sides (**Figure 3C**). The ability of the XRCC4-Fs and XRCC4-Del mutants to support LIG4-mediated ligation was indistinguishable from that of the XRCC4-Wt. Further, the activity was efficiently stimulated by XLF. We conclude that the effect of these alterations on the XRCC4/LIG4 enzyme activity is relatively minor. This finding explains the substantial complementation when the mutant proteins are exogenously expressed.

XRCC4-Fs is degraded by the proteasome.

Given the low levels of XRCC4-Fs observed in CSL16NG cells and its presence in the cytoplasm, we examined whether it is subject to proteolytic degradation. To assess this, we first transiently expressed WT and mutant XRCC4 in HEK293FT cells in the presence or absence of the protein synthesis inhibitor, cycloheximide (CHX). In the presence of CHX, XRCC4-Wt protein was stable up to 12 h, whereas XRCC4-Fs was significantly degraded (**Figure 4A**). Remarkably, the XRCC4-Del protein was as stable as XRCC4-W43R. Degradation of XRCC4-Fs was inhibited by addition of the proteasome inhibitors, MG-132 and epoxomicin (**Figure 4B**) but unaffected by the cysteine protease inhibitor E64D, which inhibits calpain and lysosomal proteases, or 3-Methyladenine (3-MA), an autophagy inhibitor (**Figure 4B**). Consistent with these observations, the level of endogenous XRCC4 in CSL16NG cells was significantly enhanced by incubation in MG132 (**Figure S8**). These findings strongly suggest that XRCC4-Fs is subjected to proteasome mediated degradation, which provides an explanation for the very low (indeed undetectable) level of the mutant XRCC4 protein and the low level of LIG4 in the patient cells. In view of these findings, we predicted that the enhanced expression of exogenous WT or mutant XRCC4 in CSL16NG cells would lead to increased LIG4 levels. Indeed, overexpression of WT and XRCC4 mutant proteins in CSL16NG resulted in recovery of LIG4 protein levels (**Figure 4C,** compare lanes 3-6 with lane 2), which is consistent with the ability of XRCC4-Fs to complement the CSL16NG repair defect.

Taking the complementation analyses and the biochemical data together, we conclude that the XRCC4-Fs mutant protein can efficiently complex with LIG4 and promote DSB rejoining and that a major impact of the change is greatly reduced

XRCC4-Fs stability due to proteasomal degradation.

The mutations in CSL16NG confer a separation of impact phenotype.

Despite the DSB repair defect observed in CSL16NG cells and marked developmental features, the patient had a normal immune response and the patient cells showed enhanced accuracy in an in vitro assay for V(D)J recombination, in marked contrast to other NHEJ-deficient patients. A trivial explanation might be that there is sufficient residual DSB repair activity to support V(D)J recombination but not the efficient repair of radiation induced DSBs. To gain further insight, we carried out a comparative analysis of the efficiency of DSB repair of CSL16NG cells and a range of patient-derived fibroblasts with deficiencies in other NHEJ proteins (XLF or LIG4) (**Figure 5A**). Since LIG4 is essential, LIG4 syndrome patients have hypomorphic mutations and hence a range of clinical severities, which generally correlate with the magnitude of the repair defect.[34] Importantly, most of the LIG4 Syndrome cells examined (and in total 7/8 lines previously examined by us) repaired most DSBs induced by 3 Gy IR by 72 h (**Figure 5A** and data not shown). (495GOS had more marked sensitivity. This line, however, had normal LIG4 protein expression, raising the possibility that the mutational change could exert a dominant negative phenotype). Except for patient 180BR,[35, 36] all showed some degree of immunodeficiency. Of relevance here, the *in vitro* ligation activities of 411BR and cell line 2303 have been previously estimated to be < 1%, yet both lines rejoin the DSBs induced by 3 Gy within 72h.[34, 37] 411BR has previously been shown to express normal levels of mutant LIG4[34, 37] but, significantly, 2303 expressed lower levels of LIG4 compared to CSL16NG (**Figures 5B and 5C**). Collectively, this analysis of LIG4 syndrome cell lines strongly

suggests that only a low level of residual LIG4 activity (1% or less) suffices to repair all DSBs induced by 3 Gy IR, albeit with slow kinetics, a conclusion consistent with previous findings.[38] In marked contrast, CSL16NG fibroblasts, despite harbouring 5-15 % residual LIG4 levels had a severe DSB repair defect. The magnitude of the DSB repair defect was similar to, although more severe than, that shown by XLF-defective cells. The repair defect was evident following exposure to a low dose of radiation (0.5 Gy) and, after 3 Gy IR, 25 % of the DSBs remained unrepaired even 8 days post exposure (**Figures S9A and S9B**). Indeed, this represents possibly the most severely DSB repair defective human cell line that we have encountered. In rodent cells, defects in NHEJ proteins, including XLF can lead to DSB repair by alternative NHEJ (Alt-NHEJ).[39] However, the residual DSB repair in CSL16NG cells is not inhibited by a PARP inhibitor, KU58958 (**Figure S9C**) and displays an additive repair defect following siRNA depletion of *LIG4* (**Figure S9D**) or the addition of a DNA-PK inhibitor NU7441 (**Figures S9C),** suggesting that it does not represent Alt-NHEJ but residual canonical NHEJ activity. This is consistent with current evidence that Alt-NHEJ does not function in human cells unless Ku is absent.[40, 41] We note also that CSL16NG cells expressed close to normal levels of XLF, as did the LIG4 syndrome cells examined (**Figure 5B**).

These findings show that CSL16NG has a very severe defect in repair of DSB and importantly, they suggest that the normal immune response of the patient cannot be attributed to a mild defect in DSB repair, providing evidence for a separation of function phenotype.

Discussion.

We describe a patient with mutational changes in the NHEJ protein, XRCC4. The patient described here has unexpected clinical features for an NHEJ deficiency. Our detailed cellular analysis provides evidence for a separation of impact phenotype, namely severely defective DSB repair but normal immune responses, and reveals a clinical and cellular manifestation for mutations in XRCC4 that is unexpected and distinct from those conferred by diminished LIG4 enzyme activity.

In patient CSL16NG, the major expressed allele encodes a protein with 68 aberrant C-terminal amino acids p.(D254fs*68). The mutant protein can interact with LIG4 and is largely functional for DSB repair *in vitro* and *in vivo*. The major impact of the mutational change is to promote proteasome mediated degradation of the mutant protein, so that CSL16NG cells have very low XRCC4 protein levels.

There are two remarkable findings from our results, with important implications. First, the defect in DSB repair is significantly greater than that of cells with lower levels of LIG4, and secondly, despite this defect, V(D)J recombination is proficient and the patient does not display any gross clinical or laboratory immunodeficiency to date. We will consider these findings in turn.

DSB repair defect. Despite low XRCC4 levels, there is ~5-15 % residual LIG4 localised in the nucleus. This residual activity, by comparison with LIG4 syndrome cells, is estimated to be sufficient to affect slow DSB rejoining after 3 Gy IR, yet CSL16NG cells have a dramatic DSB repair defect. These findings, therefore, strongly suggest that there must be a role for XRCC4 in DSB rejoining that is distinct from its accepted function in stabilising LIG4.

Recent studies have shown that XLF forms filaments with XRCC4 and

current models propose that these function in DNA end-stabilisation during DSB repair.[8, 10-12] This structural role for XRCC4 in forming filaments necessitates multiple XRCC4 molecules at each DNA end and is unlikely to be fulfilled by a low level of residual XRCC4 protein. The similar DSB repair defect between XLF-deficient and CSL16NG cells supports an overlapping role in DSB repair. Thus, we propose that the marked DSB repair defect in CSL16NG cells is a consequence of insufficient XRCC4 to form filaments with XLF. In contrast, low residual LIG4, of which only 1-2 molecules are likely to be required per DSB, is sufficient to allow complete DSB repair albeit with slow kinetics (**Figure S9B**). If this hypothesis is correct, our data provide the first evidence suggesting that XRCC4's role in XLF filament formation can be uncoupled from its more direct role in ligation.

DSB repair defect and normal immune response. Despite the marked DSB repair defect in CSL16NG cells and an altered repair pattern during CSR, the patient did not display any immunodeficiency, and in a cell based assay, V(D)J recombination took place with enhanced rather than reduced accuracy. Most LIG4 syndrome cells, including line 2303, displayed combined immunodeficiency or severe combined immunodeficiency, yet our comparative analysis of DSB repair showed that most LIG4 Syndrome cells had more efficient DSB repair than CSL16NG.[16] Thus the normal immune response of CSL16NG cannot be attributed solely to a mild DSB repair defect, suggesting a separation of impact phenotype.

This raises the intriguing possibility that XRCC4's role in complex with XLF in end-stabilisation may be dispensable for V(D)J recombination. XLF-deficient patients, however, do display immunodeficiency demonstrating a role for XLF in V(D)J recombination in humans.[18] There appear to be distinctions between the requirement for

synapsis/end-stabilisation during V(D)J recombination versus the repair of genotoxic DSBs. Indeed, XLF is dispensable for V(D)J recombination in mice where ATM, DNA-PK and 53BP1 have been proposed to have redundant roles, yet XLF deficient patients frequently display pronounced immunodeficiency.[42, 43] We note that the phenotype of CSL16NG cells overlaps with that of XLF-deficient mice (ie a marked DSB repair defect but proficient V(D)J recombination).[15] Additionally in mice, RAG2 has been proposed to have a role in influencing rejoining during V(D)J recombination.[44] We note also that a recent paper identified PAXX as a new XRCC4 super-family member that functions with XRCC4 and XLF in NHEJ.[45] It is possible that there could be redundancy between PAXX and XRCC4 during V(D)J recombination but not during the repair of genotoxic DSBs. Further work is required to gain insight into the mechanism underlying these intriguing findings.

An additional novel phenotype of CSL16NG cells is that all the junctions formed in the V(D)J recombination assay involved high fidelity joining of the coding ends. This phenotype contrasts strongly with the lack of direct rejoining of DNA ends in the NHEJ plasmid assay and the CSR junction analysis, and further supports a separation of function phenotype. The basis for the difference from control cells in the V(D)J recombination assay, where small deletions/insertions can arise is unclear. However the accurate rejoining contrasts to other NHEJ deficient lines, which are characterised by large deletions and microhomology usage. Although the lack of junctional diversity seen in this fibroblast based assay might predict a diminished repertoire of T- and B- cells, it is possible that the assay does not fully reflect the *in vivo* process due to differences between fibroblasts and lymphocytes (e.g. T-cells express tdT).

Using CSL16NG fibroblasts and the assays established here, we also examined the impact of W43R, a previously described XRCC4 mutational change observed in a patient with primordial dwarfism.[33] We provide evidence that W43R is a pathological mutational change, supporting the notion that homozygous expression of XRCC4-W43R underlies the primordial dwarfism observed in the patient.

Several recent studies have also described patients with mutations in XRCC4.[46-49] Strikingly, all patients displayed microcephaly and growth delay but no overt immunodeficiency (although detailed examination of V(D)J recombination ability was not investigated in these patients). This strengthens our proposal that XRCC4 deficiency confers a separation of impact phenotype (impacting upon the repair of genotoxic DSBs but not the repair of DSBs induced during V(D)J recombination), demonstrating that this is not a finding specific to our patient. The severe DSB repair defect in CSL16NG cells also provides a potential explanation for the marked neurological phenotype observed in the patient. An unusual feature for NHEJ deficiency was the development of progressive ataxia in the patient and it is tempting to speculate that this is a consequence of persisting unrepaired DSBs. Intriguingly, a progressive neurological phenotype involving unsteady gait was recently observed in two XRCC4-deficient siblings, who similarly had no detectable residual XRCC4 protein.[49] This supports the notion that progressive ataxia could be a consequence of marked XRCC4 deficiency.

The prediction of our working model is that mutations in *XRCC4* that result in low expression of a protein capable of interacting with LIG4 will confer marked neurological deficits without associated immune deficiency. Given the striking resemblance of patient CSL16NG, when a young child, to CS patients, *XRCC4* should be considered a candidate for potential causal mutations in further patients with similar

features, including further CS-like patients with normal transcription-coupled nucleotide excision repair.

In summary, we describe a patient with mutations in *XRCC4*. The patient had marked neurological abnormalities with progressive ataxia. Our biochemical and cellular analysis provides evidence that the mutational changes in this patient confer a separation of impact phenotype with a severe defect in DSB repair but no marked defect in V(D)J recombination. Recent papers have described additional XRCC4-deficient patients with a normal immune response.[33, 46-49] As a working model, we propose that this could arise from a separation of XRCC4 function in stabilising LIG4 versus its role in forming filaments with XLF. We propose that XRCC4 is required for all DSB rejoining since LIG4 is unstable in the absence of XRCC4. However, only a low-level of protein suffices to provide sufficient LIG4 to effect slow rejoining. In contrast, XRCC4's role in filament formation with XLF is essential for efficient rejoining of genotoxic DSBs but appears to be dispensable during V(D)J recombination in human cells, possibly due to redundancy with other proteins that can promote synapsis.

Acknowledgements

We are grateful to Elena Korneeva for technical assistance, Dik van Gent and Jean-Pierre Villartay for cell lines from patients, Hironori Niki for general discussions, and to the patient's mother for much helpful clinical information.

This work was supported by a foreign researcher grant from the Japan Society for the Promotion of Science (JSPS) (P14093) to C.G.; a grant for Research for overcoming intractable diseases (H26-general-046) from The Ministry of Health Labour and Welfare of Japan, KAKENHI Grants-in-Aid for Scientific Research (B) (26291005) from JSPS, KAKENHI Grants-in-Aid for Scientific Research (A) (Overseas Academic Research) (15H02654) from JSPS and a science research grant from the Uehara Memorial Foundation to T.O; KAKENHI Grants-in-Aid for Young Scientists (A) (15H05333) from JSPS, a research grant from the Uehara Memorial Foundation, a medical research grant from Daiichi-Sankyo Foundation of Life Science and a medical research grant from Takeda Science Foundation and Special Coordination Funds for Promoting Science and Technology from the Japan Science and Technology Agency (JST) to Y.Nakazawa; the Swedish Research Council and the European Research Council (242551-ImmunoSwitch) to Q.P-H.

References

1. Gellert M. V(D)J recombination: RAG proteins, repair factors, and regulation. Annu Rev Biochem 2002; 71:101-32.
2. Alt FW, Zhang Y, Meng FL, Guo C, Schwer B. Mechanisms of programmed DNA lesions and genomic instability in the immune system. Cell 2013; 152:417-29.

3. Boboila C, Alt FW, Schwer B. Classical and alternative end-joining pathways for repair of lymphocyte-specific and general DNA double-strand breaks. Advances in immunology 2012; 116:1-49.
4. Radhakrishnan SK, Jette N, Lees-Miller SP. Non-homologous end joining: emerging themes and unanswered questions. DNA Repair (Amst) 2014; 17:2-8.
5. Critchlow SE, Bowater RP, Jackson SP. Mammalian DNA double-strand break repair protein XRCC4 interacts with DNA ligase IV. Current Biology 1997; 7:588-98.
6. Grawunder U, Zimmer D, Fugmann S, Schwarz K, Lieber MR. DNA ligase IV is essential for V(D)J recombination and DNA double-strand break repair in human precursor lymphocytes. Molecular Cell 1998; 2:477-84.
7. Mani RS, Yu Y, Fang S, Lu M, Fanta M, Zolner AE, et al. Dual modes of interaction between XRCC4 and polynucleotide kinase/phosphatase: implications for nonhomologous end joining. J Biol Chem 2010; 285:37619-29.
8. Hammel M, Rey M, Yu Y, Mani RS, Classen S, Liu M, et al. XRCC4 protein interactions with XRCC4-like factor (XLF) create an extended grooved scaffold for DNA ligation and double strand break repair. The Journal of biological chemistry 2011; 286:32638-50.
9. Williams GJ, Hammel M, Radhakrishnan SK, Ramsden D, Lees-Miller SP, Tainer JA. Structural insights into NHEJ: building up an integrated picture of the dynamic DSB repair super complex, one component and interaction at a time. DNA Repair (Amst) 2014; 17:110-20.
10. Mahaney BL, Hammel M, Meek K, Tainer JA, Lees-Miller SP. XRCC4 and XLF form long helical protein filaments suitable for DNA end protection and alignment to facilitate DNA double strand break repair. Biochemistry and cell biology = Biochimie et biologie cellulaire 2013; 91:31-41.
11. Andres SN, Vergnes A, Ristic D, Wyman C, Modesti M, Junop M. A human XRCC4-XLF complex bridges DNA. Nucleic Acids Res 2012;

40:1868-78.
12. Wu Q, Ochi T, Matak-Vinkovic D, Robinson CV, Chirgadze DY, Blundell TL. Non-homologous end-joining partners in a helical dance: structural studies of XLF-XRCC4 interactions. Biochem Soc Trans 2011; 39:1387-92, suppl 2 p following 92.
13. Barnes DE, Stamp G, Rosewell I, Denzel A, Lindahl T. Targeted disruption of the gene encoding DNA ligase IV leads to lethality in embryonic mice. Curr Biol 1998; 8:1395-8.
14. Frank KM, Sekiguchi JM, Seidl KJ, Swat W, Rathbun GA, Cheng HL, et al. Late embryonic lethality and impaired V(D)J recombination in mice lacking DNA ligase IV. Nature 1998; 396:173-7.
15. Li G, Alt FW, Cheng HL, Brush JW, Goff PH, Murphy MM, et al. Lymphocyte-specific compensation for XLF/cernunnos end-joining functions in V(D)J recombination. Mol Cell 2008; 31:631-40.
16. O'Driscoll M, Cerosaletti KM, Girard P-M, Dai Y, Stumm M, Kysela B, et al. DNA Ligase IV mutations identified in patients exhibiting development delay and immunodeficiency. Mol Cell 2001; 8:1175-85.
17. Woodbine L, Neal JA, Sasi NK, Shimada M, Deem K, Coleman H, et al. PRKDC mutations in a SCID patient with profound neurological abnormalities. J Clin Invest 2013; 123:2969-80.
18. Buck D, Malivert L, de Chasseval R, Barraud A, Fondaneche MC, Sanal O, et al. Cernunnos, a novel nonhomologous end-joining factor, is mutated in human immunodeficiency with microcephaly. Cell 2006; 124:287-99.
19. Murray JE, Bicknell LS, Yigit G, Duker AL, van Kogelenberg M, Haghayegh S, et al. Extreme growth failure is a common presentation of ligase IV deficiency. Hum Mutat 2014; 35:76-85.
20. Woodbine L, Gennery AR, Jeggo PA. The clinical impact of deficiency in DNA non-homologous end-joining. DNA Repair (Amst) 2014; 16C:84-96.
21. Kashiyama K, Nakazawa Y, Pilz DT, Guo C, Shimada M, Sasaki K, et al. Malfunction of nuclease ERCC1-XPF results in diverse clinical manifestations and causes Cockayne syndrome, xeroderma

688 pigmentosum, and Fanconi anemia. Am J Hum Genet 2013; 92:807-19.
689 22. Jia N, Nakazawa Y, Guo C, Shimada M, Sethi M, Takahashi Y, et al. A
690 rapid, comprehensive system for assaying DNA repair activity and
691 cytotoxic effects of DNA-damaging reagents. Nat Protoc 2015;
692 10:12-24.
693 23. Verkaik NS, Esveldt-van Lange RE, van Heemst D, Bruggenwirth HT,
694 Hoeijmakers JH, Zdzienicka MZ, et al. Different types of V(D)J
695 recombination and end-joining defects in DNA double-strand break
696 repair mutant mammalian cells. Eur J Immunol 2002; 32:701-9.
697 24. Du L, Peng R, Bjorkman A, Filipe de Miranda N, Rosner C, Kotnis A,
698 et al. Cernunnos influences human immunoglobulin class switch
699 recombination and may be associated with B cell lymphomagenesis. J
700 Exp Med 2012; 209:291-305.
701 25. Stavnezer J, Bjorkman A, Du L, Cagigi A, Pan-Hammarstrom Q.
702 Mapping of switch recombination junctions, a tool for studying DNA
703 repair pathways during immunoglobulin class switching. Adv
704 Immunol 2010; 108:45-109.
705 26. Pan Q, Petit-Frere C, Dai S, Huang P, Morton HC, Brandtzaeg P, et al.
706 Regulation of switching and production of IgA in human B cells in
707 donors with duplicated alpha1 genes. Eur J Immunol 2001;
708 31:3622-30.
709 27. Riballo E, Woodbine L, Stiff T, Walker SA, Goodarzi AA, Jeggo PA.
710 XLF-Cernunnos promotes DNA ligase IV-XRCC4 re-adenylation
711 following ligation. Nucleic Acids Res 2009; 37:482-92.
712 28. Neilan EG, Delgado MR, Donovan MA, Kim SY, Jou RL, Wu BL, et al.
713 Response of motor complications in Cockayne syndrome to
714 carbidopa-levodopa. Arch Neurol 2008; 65:1117-21.
715 29. Wu PY, Frit P, Meesala S, Dauvillier S, Modesti M, Andres SN, et al.
716 Structural and functional interaction between the human DNA repair
717 proteins DNA ligase IV and XRCC4. Molecular and cellular biology
718 2009; 29:3163-72.
719 30. Modesti M, Junop MS, Ghirlando R, van de Rakt M, Gellert M, Yang W,
720 et al. Tetramerization and DNA ligase IV interaction of the DNA

721 double-strand break repair protein XRCC4 are mutually exclusive. J
722 Mol Biol 2003; 334:215-28.
723 31. Dai Y, Kysela B, Hanakahi LA, Manolis K, Riballo E, Stumm M, et al.
724 Nonhomologous end joining and V(D)J recombination require an
725 additional factor. Proc Natl Acad Sci U S A 2003; 100:2462-7.
726 32. Pan-Hammarstrom Q, Jones AM, Lahdesmaki A, Zhou W, Gatti RA,
727 Hammarstrom L, et al. Impact of DNA ligase IV on nonhomologous
728 end joining pathways during class switch recombination in human
729 cells. J Exp Med 2005; 201:189-94.
730 33. Shaheen R, Faqeih E, Ansari S, Abdel-Salam G, Al-Hassnan ZN,
731 Al-Shidi T, et al. Genomic analysis of primordial dwarfism reveals
732 novel disease genes. Genome Res 2014; 24:291-9.
733 34. Girard PM, Kysela B, Harer CJ, Doherty AJ, Jeggo PA. Analysis of
734 DNA ligase IV mutations found in LIG4 syndrome patients: the impact
735 of two linked polymorphisms. Hum Mol Genet 2004; 13:2369-76.
736 35. Riballo E, Critchlow SE, Teo SH, Doherty AJ, Priestley A, Broughton B,
737 et al. Identification of a defect in DNA ligase IV in a radiosensitive
738 leukaemia patient. Curr Biol 1999; 9:699-702.
739 36. Riballo E, Doherty AJ, Dai Y, Stiff T, Oettinger MA, Jeggo PA, et al.
740 Cellular and biochemical impact of a mutation in DNA ligase IV
741 conferring clinical radiosensitivity. J Biol Chem 2001; 276:31124-32.
742 37. O'Driscoll M, Cerosaletti KM, Girard PM, Dai Y, Stumm M, Kysela B,
743 et al. DNA ligase IV mutations identified in patients exhibiting
744 developmental delay and immunodeficiency. Mol Cell 2001; 8:1175-85.
745 38. Windhofer F, Wu W, Iliakis G. Low levels of DNA ligases III and IV
746 sufficient for effective NHEJ. J Cell Physiol 2007; 213:475-83.
747 39. Deriano L, Roth DB. Modernizing the nonhomologous end-joining
748 repertoire: alternative and classical NHEJ share the stage. Annu Rev
749 Genet 2013; 47:433-55.
750 40. Ghezraoui H, Piganeau M, Renouf B, Renaud JB, Sallmyr A, Ruis B, et
751 al. Chromosomal translocations in human cells are generated by
752 canonical nonhomologous end-joining. Mol Cell 2014; 55:829-42.
753 41. Oh S, Harvey A, Zimbric J, Wang Y, Nguyen T, Jackson PJ, et al. DNA

754 ligase III and DNA ligase IV carry out genetically distinct forms of end
755 joining in human somatic cells. DNA Repair (Amst) 2014; 21:97-110.
756 42. Zha S, Guo C, Boboila C, Oksenych V, Cheng HL, Zhang Y, et al. ATM
757 damage response and XLF repair factor are functionally redundant in
758 joining DNA breaks. Nature 2011; 469:250-4.
759 43. Liu S, Opiyo SO, Manthey K, Glanzer JG, Ashley AK, Amerin C, et al.
760 Distinct roles for DNA-PK, ATM and ATR in RPA phosphorylation and
761 checkpoint activation in response to replication stress. Nucleic Acids
762 Res 2012; 40:10780-94.
763 44. Gigi V, Lewis S, Shestova O, Mijuskovic M, Deriano L, Meng W, et al.
764 RAG2 mutants alter DSB repair pathway choice in vivo and illuminate
765 the nature of 'alternative NHEJ'. Nucleic Acids Res 2014; 42:6352-64.
766 45. Ochi T, Blackford AN, Coates J, Jhujh S, Mehmood S, Tamura N, et al.
767 DNA repair. PAXX, a paralog of XRCC4 and XLF, interacts with Ku to
768 promote DNA double-strand break repair. Science 2015; 347:185-8.
769 46. Rosin N, Elcioglu NH, Beleggia F, Isguven P, Altmuller J, Thiele H, et
770 al. Mutations in XRCC4 cause primary microcephaly, short stature
771 and increased genomic instability. Hum Mol Genet 2015.
772 47. Murray JE, van der Burg M, H IJ, Carroll P, Wu Q, Ochi T, et al.
773 Mutations in the NHEJ component XRCC4 cause primordial dwarfism.
774 Am J Hum Genet 2015; 96:412-24.
775 48. de Bruin C, Mericq V, Andrew SF, van Duyvenvoorde HA, Verkaik NS,
776 Losekoot M, et al. An XRCC4 splice mutation is associated with severe
777 short stature, gonadal failure, and early-onset metabolic syndrome. J
778 Clin Endocrinol Metab 2015:jc20151098.
779 49. Bee L, Nasca A, Zanolini A, Cendron F, d'Adamo P, Costa R, et al. A
780 nonsense mutation of human XRCC4 is associated with adult-onset
781 progressive encephalocardiomyopathy. EMBO Mol Med 2015.
782 50. Frank KM, Sharpless NE, Gao Y, Sekiguchi JM, Ferguson DO, Zhu C,
783 et al. DNA ligase IV deficiency in mice leads to defective neurogenesis
784 and embryonic lethality via the p53 pathway. Mol Cell 2000;
785 5:993-1002.
786 51. Enervald E, Du L, Visnes T, Bjorkman A, Lindgren E, Wincent J, et al.

A regulatory role for the cohesin loader NIPBL in nonhomologous end joining during immunoglobulin class switch recombination. J Exp Med 2013; 210:2503-13.

52. Nakazawa Y, Yamashita S, Lehmann AR, Ogi T. A semi-automated non-radioactive system for measuring recovery of RNA synthesis and unscheduled DNA synthesis using ethynyluracil derivatives. DNA Repair (Amst) 2010; 9:506-16.

53. Limsirichaikul S, Niimi A, Fawcett H, Lehmann A, Yamashita S, Ogi T. A rapid non-radioactive technique for measurement of repair synthesis in primary human fibroblasts by incorporation of ethynyl deoxyuridine (EdU). Nucleic Acids Res 2009; 37:e31.

Figure legends

Figure 1. Identification of mutations in the *XRCC4* gene in CSL16NG

(A) Clinical pictures of CSL16NG at age 1.5, 16 and 23 (with informed written consent from the patient's mother). (B) Immunoblotting of XRCC4 and LIG4 proteins in CSL16NG and HCT116-XRCC4 (-/-) cells as well as normal 48BR, 1BR.3 and HCT116 cells with alpha-tubulin as a loading control. The black solid arrows indicate the position of each protein. The dilutions indicate that the amount of XRCC4 in the patient cells is < 2% (detection limit) of normal cells. (C) Immunoblots showing the expression of LIG4 proteins in normal (48BR), patient (CSL16NG) and N114P2 (LIG4 -/-) fibroblasts. (D) Immunofluorescent staining of endogenous XRCC4 protein in normal 48BR, CSL16NG cells. Cells were fixed and immunostained with mouse anti-XRCC4 antibody (C4, Green). DAPI, DAPI staining (Blue); Merge, merged picture; Scale bar, 20 μm.

Figure 2. CSL16NG defects in DNA double strand break repair

(A) The colony-forming ability of primary CSL16NG cells was compared with that of a normal control (1BR.3) and that of a *LIG4*-defective F07/614 cells after treatment with different doses of γ-ray. The range of sensitivity displayed by another healthy individual and 20 other individuals deemed to have a normal (or close to normal) response is shown in **Figure S4**. In (A), all primary cell lines used were between 5 and 9 passages following establishment from a skin biopsy. Error bars represent S.D. obtained from triplicate experiments. (B) CSL16NG cell sensitivity to γ-ray was rescued by overexpression of the WT XRCC4 protein. Cell proliferation 24 hrs after γ-irradiation was determined by EdU incorporation and compared with that in unirradiated cells. (C) Complementation of the DSB repair defect in CSL16NG cells. CSL16NG cells stably expressing the V5-tagged WT XRCC4 or the indicated mutant XRCC4 proteins were irradiated with 3 Gy IR. DSB repair kinetics was measured as described above. In (B,C), primary cell lines used were between 16 and 20 passages following establishment from a skin biopsy. Error bars represent S.D. obtained from triplicate experiments.

Figure 3. The XRCC4-Fs-DNA ligase IV complex has normal ligase activity

(A) His-tagged LIG4 and the FLAG-tagged WT and the mutant XRCC4 proteins were expressed in HEK293FT cells. Total cell lysates were prepared and the XRCC4-DNA ligase IV complexes were purified on anti-FLAG M2 beads as described in **Materials and Methods**. Purified proteins were run on a SDS-PAGE and either stained with Coomassie brilliant blue (left panel) or immunoblotted with antibodies against LIG4 or XRCC4 as indicated (right panel). (B) GST-tagged XLF was purified from *E. coli* BL21 according to the methods described previously.[27] (C) The purified XRCC4-DNA ligase

838 IV complexes and XLF were incubated with the indicated Cy5-labeled and non-labeled
839 dsDNA substrates. Ligated products diagrammed at right of figure were identified on
840 1 % agarose gel electrophoresis by their decreased mobility.
841
842 **Figure 4. XRCC4-Fs mutant protein is unstable in cells**
843 (A) Immunoblots of the WT and mutant XRCC4 proteins with CHX (100 μg/ml). (B)
844 Effects of various chemical compounds on degradation of the XRCC4-Fs protein.
845 HEK293FT cells were transiently transfected with the XRCC4-Fs cDNA and treated
846 with cycloheximide together with proteasome inhibitors, MG132 (20 μM) or
847 epoxomicin (1 μM), protease inhibitor E64D (20 μM), or autophagy inhibitor 3-MA (10
848 mM) for the indicated period. DMSO was used as a vehicle control. (C) Overexpression
849 the WT and the mutant XRCC4 proteins restored LIG4 expression levels. V5-tagged
850 XRCC4-Wt or mutant proteins were ectopically expressed in CSL16NG cells and the
851 levels of LIG4 were analysed by immunoblotting with two different antibodies.
852
853 **Figure 5. CSL16NG cells show an exceptionally marked DSB repair defect.**
854 (A) Double strand break (DSB) repair kinetics following γ-irradiation were determined
855 in normal and various DSB-repair deficient patient cell lines. Residual DSBs were
856 measured by enumeration of the average number of γH2AX foci at each indicated time
857 point. (B) Immunoblots showing the expression of XRCC4, LIG4 and XLF proteins in
858 cells from normal individuals (1BR.3), patient (CSL16NG) as well as previously
859 reported XLF-patient (2BN) and LIG4-patients (F07/614 and 2303). (C) Diminished
860 expression of the LIG4 in CSL16NG cells were confirmed by immunofluorescent
861 staining. DAPI, DAPI (Blue). All primary fibroblasts used were between 5 and 9

passages following establishment from a skin biopsy. Error bars represent S.D. obtained from triplicate experiments.

Table 1. Increased microhomology-dependent repair in CSL16NG ells in plasmid-based NHEJ assay[a]

Cell line	Direct end-joining	6bp MH	Deletion+MH	Deletion only	Total No. of junctions
CSL16NG	**1 (2%)***↓**	**47 (78%)***↑**	3 (5%)	9 (15%)	60
XLF$^{-/-}$[b]	**3 (4%)***↓**	**55 (81%)***↑**	10 (15%)	**0 (0%)**↓**	68
411BR LIG4d[c]	**4 (22%)***↓**	**12 (67%)***↑**	0 (0%)	2 (11%)	18
Controls[d]	105 (72%)	11 (8%)	14 (10%)	16 (11%)	146

a. Statistical calculations performed by χ^2 test. Significant changes are indicated in bold. **p*<0.05, ***p*<0.01, ****p*<0.001

b. Previously published results from XLF-deficient cell line.[24]

c. 411BR, described in.[16, 50]

d. Newly generated results merged with previously published results from control cell line.[24, 51]

Table 2. Increased fidelity of end joining at coding junctions in CSL16NG in plasmid-based VDJ-assay[a]

Cell line	Accurate end-joining	4bp MH	Deletion+MH	Deletion only	Total No. of junctions
CSL16NG	**18 (90%)***↑	**0 (0%)***↓	**2 (10%)****↓	**0 (0%)***↓	20
XLF$^{-/-}$	5 (12%)	4 (10%)	**32 (78%)***↑	**0 (0%)***↓	41
Controls	13 (10%)	25 (20%)	57 (46%)	30 (24%)	125

a. Statistical calculations performed by χ^2 test. Significant changes are indicated in bold.

*p<0.05, **p<0.01, ***p<0.001

Table 3. Characterization of Sμ-Sα junctions[a]

Patients	Perfectly matched short homology						Total No. of S fragments
	0 bp		1-3 bp	4-6 bp	7-9 bp	≥ 10 bp	
	Direct end-joining	Small insertions					
CSL16NG (n=1)	1 (5%)	2 (9%)	4 (18%)	2 (9%)	**5 (23%)*↑**	**8 (36%)***↑**	22
LIG4d[b] (n=2)	**0 (0%)*↓**	**1 (3%)**↓**	7 (23%)	4 (13%)	4 (13%)	**14 (47%)***↑**	30
Controls[b] (n=17)	28 (18%)	39 (25%)	56 (36%)	15 (10%)	11 (7%)	5 (3%)	154

a. Statistical analysis was performed using χ^2 test and significant differences are indicated in bold. * $p<0.05$, ** $p<0.01$, *** $p<0.001$.

b. Previously published junctions from *LIG4*-deficient patients and controls.[32]

n= Indicates number of individuals in each group.

Supplemental Materials

Supplemental methods

RRS, UDS and RDS assays

Detailed experimental procedures have been described previously.[22, 52, 53] Briefly, normal 48BR, CSL16NG and XPA patient-derived primary fibroblasts (XP15BR) were seeded in 96-well plates (BD Falcon). For RRS assay, cells were UV-irradiated (254 nm UVC, 12 J/cm^2) and incubated for 12 hours for RNA synthesis recovery, followed by ethynyluridine (EU) incorporation. For the UDS and RDS assays, UV- or γ-ray irradiated cells were immediately incubated with 5'-ethynyl-2'-deoxyuridine (EdU) for measuring repair synthesis. After incorporation of EdU or EU, cells were fixed, followed by Alexa Fluor 488-azide coupling and DAPI staining. Image acquisition and data processing were automated using the Cellomics ArrayScan VTI (Thermo Scientific).

Identification of the pathogenic mutations by exome sequencing

We performed exome sequencing of the patient, CSL16NG, using the Agilent SureSelect Exome Target Enrichment System (version.5 50Mbp target), followed by paired-end sequencing (101 bp/read) on the Illumina Hiseq 2500 sequencer. We obtained ~193 million reads (~ 19 Giga base pairs). Of the QC-passed initial sequencing reads, 18.4 Gbp are uniquely mapped to the human reference sequence (b37). Of the mapped sequences, 12.9 Gbp (66.33%) are further mapped to the target exon regions with a mean coverage of 89.05x. 98.8% of the target bases were read more than 2x coverage. We identified a total of 740,166 single nucleotide variants (SNVs) and 88,210 insertions and deletions (indels). To identify potential pathogenetic changes, we firstly

determined 'functionally significant variants', which are coding non-synonymous SNVs, stopgains and stoplosses, splice-site variants, and coding indels. We identified 11,505 functionally significant variants. The identified variants were then filtered out to extract 'novel functionally significant variants'. We compared the identified variants with dbSNP137, 1000 Genomes Project, and 88 in-house exome sequencing data. Variants found in these databases were excluded. As a consequence of these filtering process, totally 140 novel functionally significant variants were determined. Based on a recessive inheritance model, we found 5 pathogenic candidate genes in the patient (**Table S1**).

Table S1. Novel homozygous and compound heterozygous variants in the candidate genes identified by the exome sequencing of the patients CSL16NG.

Patient	Chr.	Position	Genotype	Gene	Mutation type	Nucleotide change	Amino-acid change
CSL16NG	3	184104702	Het	*CHRD*	ns	c.G2266A	p.D756N
CSL16NG	3	184103873	Het	*CHRD*	ns	c.C1858T	p.R620W
CSL16NG	**5**	**82554363**	**Het**	***XRCC4***	**fs del**	**c.760delG**	**p.D254fs**
CSL16NG	**5**	**82500668**	**Het**	***XRCC4***	**sg**	**c.673T**	**p.R225***
CSL16NG	9	35906600	Hom	*HRCT1*	fs ins	c.316_317insA	p.P106fs
CSL16NG	11	1266064	Het	*MUC5B*	ns	c.A7963G	p.I2655V
CSL16NG	11	1247871	Het	*MUC5B*	ns	c.G226T	p.V76L
CSL16NG	19	1863385	Hom	*KLF16*	ns	c.G112A	p.A38T

Abbreviations used in this table: Chr., chromosome; Position, refseq position of the variant; Genotype, Hom / homozygous, Het / heterozygous; Gene, gene symbol in which the variant is located; Mutation type, ns / nonsynonymous missense, fs del / frameshift deletion, fs ins / frameshift insertion, sg / stop gain; Nucleotide change, base change and base number resulting from the observed variant; Amino acid change, amino acid change and codon number resulting from the observed variant.

Table S2. Blood immunological tests on CSL16NG

Immunological parameter	Value	Age-related normal range
CD3	1973 cells/μl	(690-2540)
CD4	1210 cells/μl	(410-1590)
CD8	744 cells/μl	(190-1140)
CD19	615 cells/μl	(90-660)
CD16/56	1506 cells/μl	(90-590)
CD45RACD27	200 cells/μl	
TCRαβ	98%	
TCRγδ	2%	
CD27-IgM+IgD+	85%	
CD27+IgM+IgD+	5%	
CD27+IgM-IgD-	7%	
IgM	1.66 g/L	(0.71-2.30)
IgA	1.26 g/L	(0.64-2.97)
IgG	7.7 g/L	(5.8-15.4)

Table S3. Primers used for allele-specific amplification.

Primer designation	Primer sequence
XRCC4-F	5’-GTGTGAGTGCTAAGGAAGCTTTGG-3’
XRCC4-WT-R	5’-TACTCTCATCATAGACTGGATCTCG-3’
XRCC4-ter-R	5’-TACTCTCATCATAGACTGGATCTCA-3’
XRCC4-com-R	5’-GTACTCTCATCATAGACTGGATCTC-3’
XRCC4-R	5’-CTTCTGGGCTGCTGTTTCTCAGAG-3’
XRCC4-WT-F	5’-TTCAGCTGCTGTAAGTAAAG-3’
XRCC4-fs-F	5’-TTCAGCTGCTGTAAGTAAAA-3’
XRCC4-com-F	5’-CTTCAGCTGCTGTAAGTAAA-3’

Supplemental Figures

Figure S1 Construction of XRCC4 mutants

(A) Sequence validation of constructed *pLenti-6.3-XRCC4-Del* and *pLenti-6.3-XRCC4-Fs* plasmid DNA. Red arrows indicated mutation sites. (B) Sequence validation of constructed *pLenti-6.3-XRCC4-W43R* plasmid DNA.

Figure S2. CSL16NG cells display normal NER activity

(A) Recovery of RNA synthesis (RRS) and (B) unscheduled DNA synthesis (UDS) are normal in CSL16NG. Nucleotide excision repair (NER)-proficient normal 48BR and -deficient XP15BR cells were used as controls. (XP represents xeroderma pigmentosum, a human disorder caused by NER-deficiency. XP causes sensitivity to ultraviolet (UV) irradiation and not to ionising radiation). Filled bars, 12 J/m^2 of 254 nm UV-C; open bars, no UV. (C) UV-sensitivity of different cell strains was determined after different doses of UVC irradiation, and their viability measured by their ability to incorporate EdU (5 μM, 1 h incubation) 24 hours after treatment. (D) Normal expression levels of the CSB and XPG proteins in CSL16NG cells. (E) Quantitation of data in (D). N.S., no statistically significant difference. All primary cell lines used were between 16 and 20 passages following establishment from a skin biopsy.

Figure S3. Expression of the *XRCC4* pathogenic alleles in CSL16NG cells

(A) Capillary Sanger sequencing confirmed that the patient is compound heterozygous for the c.673C>T in *XRCC4* exon 6, resulting in the premature stopgain p.R225* (inherited from the mother) as well as for the c.760delG in *XRCC4* exon 7, causing the frameshift p.D254fs*68 (inherited from the father). The altered amino acids are shown

in red. (B) Locations of the primer sets used for the qRT-PCR experiments are depicted. (C) Selective quantitative amplification of the WT and the mutational p.Arg225* *XRCC4* alleles in CSL16NG, and normal 48BR cells. Allele-specific primers selectively amplify the WT (c.673C) allele (XRCC4-F and XRCC4-WT-R, left panel), the pathogenic mutant (c.673C>T) allele (XRCC4-F and XRCC4-ter-R, middle panel), and both alleles at once (XRCC4-F and XRCC4-com-R, right panel). (D) Selective quantitative amplification of the WT and the mutational p.Asp254fs*68 *XRCC4* alleles in CS16LNG, and normal 48BR cells. Allele-specific primers selectively amplify the WT (c.760G) (XRCC4-WT-F and XRCC4-R, left panel), the pathogenic mutant (c.760del) allele (XRCC4-fs-F and XRCC4-R, middle panel), and both alleles at once (XRCC4-com-F and XRCC4-R, right panel). Transcripts from the *HPRT1* gene were used as a quantification control. All primary cell lines used were between 16 and 20 passages following establishment from a skin biopsy.

Figure S4 Range of radiosensitivity observed in normal patients.

Figure 2A shows the sensitivity of CSL16NG primary fibroblasts relative to control cells. To confirm that the sensitivity of CSL16NG cells lies outside of the normal range, we firstly compared the sensitivity to 1BR.3 and 48BR primary fibroblasts, both of which are derived from a healthy individual. The sensitivity of 48BR cells was similar to that shown by 1BR.3 cells. To assess the magnitude of sensitivity of a broader range of individuals, we included the analysis of the most recent 20 primary fibroblasts lines from individuals whose cells were sent to our laboratory for analysis. These individuals had a range of clinical features, including aspects of immunodeficiency. We excluded all cell lines where we had an identified genetic defect. Since these cell lines were from

non-healthy individuals, we excluded the two most sensitive lines, considering that they might be from individuals with minor genetic defects affecting radiosensitivity, resulting in the analysis of 90% of this patient subset, which we considered might represent the response of a 90% percentile. The figure shows the range of sensitivity displayed by these 18 cell lines. The response of 1BR.3 and 48BR lies within this range. The lower edge of this range may be slightly more sensitive than the true responses of healthy individuals since our 18 patients were individuals with health issues. CSL16NG cells were substantially outside of this normal range.

Figure S5. Increased microhomology usage at Sμ-Sα junctions from CSL16NG

(A) Schematic picture showing regions encoding IgM (Cμ) and IgA (Cα) on IGH locus. An Sμ-Sα junction created after switching from IgM to IgA is depicted below. (B) Switch fragments from either control (C369) or patient (CSL16NG) aligned with germline Sμ and Sα sequences are shown. Determination of repair pattern was performed as previously described.[25]. Repair by direct end-joining is designated by straight line, small insertion is underlined and microhomology-based end-joining is marked by a box. The positions of break points in germline S regions are indicated by ▼ or ▲.

Figure S6 Ectopic expression of the XRCC4 mutant proteins

(A) Schematic representation of human full-length XRCC4 and XRCC4 mutants used for the complementation analyses. The light blue box indicates an aberrant C-terminal 68 amino acids (aa). (B) Percentages of XRCC4 expressing cells were confirmed by immunofluorescent staining of the V5-tagged proteins.

Figure S7. ***XRCC4*** **cDNA complements the DSB repair defect (53BP1)**

(A, B) 1BR.3 normal, and CSL16NG hTERT immortalized fibroblasts were transfected with GFP-tagged full-length *XRCC4* cDNA (XRCC4-Wt) or mutant XRCC4 (XRCC4-Fs). 24 hours after transfection, cells were irradiated with 3 Gy γ-rays, and the number of 53BP1 foci in GFP-positive cells was enumerated at 0.25 and 8 hours. Substantial correction of the DSB repair defect of patient cells was observed upon expression of both WT and mutant *XRCC4* cDNA. No correction was observed after transfection of *XRCC4* cDNA into *LIG4*-defective cells. BG, background (no irradiation); Error bars, S.D. of mean of triplicate experiments. In this experiment, the green channel detected both 53BP1 + GFP-tagged XRCC4. It was possible to identify defined 53BP1 foci above the background GFP signals of transfected cells although this is difficult to convey in the images. 53BP1 foci were enumerated in untransfected (low pan nuclear GFP signal) and in transfected (high pan nuclear signal) cells. Untransfected 1BR.3 cells have a strong XRCC4 signal, some residual 53BP1 foci at 8 h post 3 Gy and little background GFP signal. Untransfected CSL16NG cells have a low XRCC4 signal, elevated 53BP1 foci compared to 1BR.3 cells. Transfected CSL16NG cells expressing WT-XRCC4 have close to a WT level of XRCC4, reduced residual 53BP1 foci and strong GFP pan nuclear staining. Transfected CSL16NG cells expressing XRCC4-Fs showed a good nuclear staining of XRCC4 as well as some cytoplasmic staining, a strong pan nuclear signal of GFP and a number of 53BP1 foci that was slightly higher than that shown in cells expressing WT-XRCC4. The enumeration of 53BP1 foci in untransfected 1BR.3 or CSL16NG cells was similar to that observed in other experiments using these cells.

Figure S8. Proteasomal degradation of the endogenous XRCC4-Fs mutant protein

(A) Normal 48BR and CSL16NG cells were treated with CHX (100 μg/ml), MG132 (20 μM), or with epoxomicin (1 μM) for 12 hours. Immunofluorescent staining was conducted using mouse anti-XRCC4 antibody (C4, Green). DAPI, DAPI staining (Blue); Merge, merged picture; Alexa 488 only, staining only with Alexa fluor 488-conjugated secondary antibody; Scale bar, 100 μm. (B) 48BR and CSL16NG cells were treated with MG132 (20 μM) for 12 hours, the total cell lysates were subjected to SDS-PAGE and Western Blotting analysis using anti-XRCC4 or anti-DNA Ligase IV antibodies.

Figure S9. CSL16NG defects in DSB repair

(A) Normal 1BR.3 and CSL16NG primary fibroblasts were irradiated with 0.5 Gy γ-ray. The average number of γH2AX foci was enumerated at the indicated times. Results represent the mean +/- S.D. of 3 experiments. (B) Normal 48BR, CSL16NG, 2BN (XLF-defective) and 2303 (LIG4 syndrome) cells were untreated or treated with 3 Gy γ-ray and incubated for 8 days to allow DSB repair. γH2AX foci were enumerated at the indicated times. Results represent the mean +/- S.D. of 3 experiments (C) Normal 48BR and CSL16NG cells were treated with 3 Gy γ-irradiation and incubated with or without the 0.5 μM PARP inhibitor (KU58958, a kind gift from AstraZeneca) or 5 mM DNA-PK inhibitor (NU7441, Stratech Scientific, UK) for the indicated times. (D) Left panel, knockdown of *LIG4* in CSL16NG hTERT cells shows an additive DSB repair defect demonstrating that there is residual NHEJ activity. "+ LigIV kd" represents

knockdown of *LIG4* prior to IR and γH2AX analysis; Right panel images show two cells (top image, DAPI; 2nd image, γH2AX; 3rd and 4th image, LIG4). The cell with a solid asterisk has undergone knockdown, the other has not. The cell with knockdown has a greater level of DSBs remaining as shown by intense γH2AX staining. The bottom image has been amplified to show enhanced intensity of staining. This image shows that even in the knocked down CSL16NG hTERT cells, there is residual detectable LIG4. Thus, the residual DSB rejoining is most likely still attributable to residual NHEJ. All primary cell lines used were between 5 and 9 passages following establishment from a skin biopsy. Error bars in panels A and B represent S.D. obtained from triplicate experiments. Where only two experiments were carried out (C and D) individual experiments have been plotted side by side.

XRCC4-deficiency in humans causes a marked neurological phenotype but no overt immunodeficiency

Chaowan Guo[1,2,3,11], Yuka Nakazawa[1,2,3,11], Lisa Woodbine[4,11], Andrea Björkman[5], Mayuko Shimada[2,3], Heather Fawcett[4], Nan Jia[1,2,3], Kaname Ohyama[2,6], Taosheng Li[7], Yuji Nagayama[3], Norisato Mitsutake[2,8], Qiang Pan-Hammarström[5], Andrew R Gennery[9], Alan R Lehmann[4], Penny A Jeggo[4,*], Tomoo Ogi[1,2,3,10,*]

[1]Department of Genetics, Research Institute of Environmental Medicine (RIeM), Nagoya University, Furo-cho, Chikusa-ku, Nagoya, 464-8601, Japan; [2]Nagasaki University Research Centre for Genomic Instability and Carcinogenesis (NRGIC), 1-12-4, Sakamoto, Nagasaki, 852-8523 Japan; [3]Department of Molecular Medicine, Atomic Bomb Disease Institute, Nagasaki University, 1-12-4 Sakamoto, Nagasaki, 852-8523, Japan; [4]Genome Damage and Stability Centre, University of Sussex, Falmer, Brighton, BN1 9RQ, United Kingdom; [5]Department of Laboratory Medicine, Karolinska Institutet, Karolinska University Hospital, Huddinge, SE-14186 Stockholm, Sweden; [6]Course of Pharmaceutical Sciences, Graduate School of Biomedical Sciences, Nagasaki University, 1-14, Bunkyo, Nagasaki 852-8521 Japan. [7]Department of Stem Cell Biology, Atomic Bomb Disease Institute, Nagasaki University, 1-12-4, Sakamoto, Nagasaki, 852-8523 Japan; [8]Department of Radiation Medical Sciences, Atomic Bomb Disease Institute, Nagasaki University, 1-12-4 Sakamoto, Nagasaki, 852-8523, Japan; [9]Institute of Cellular Medicine, Newcastle University, Newcastle upon Tyne Hospitals NHS Foundation Trust, Newcastle upon Tyne, United Kingdom; [10]Microbial Genetics Laboratory, Genetic

24 Strains Research Center, National Institute of Genetics, 1111 Yata, Mishima 411-8540,
25 Japan; [11]These authors contributed equally to this work.
26
27 *Correspondence: togi@riem.nagoya-u.ac.jp (T.O), p.a.jeggo@sussex.ac.uk (P.A.J.)
28

Abstract

Background: Non-homologous end-joining (NHEJ) is the major DNA double strand break (DSB) repair mechanism in human cells. The final rejoining step requires DNA ligase IV (LIG4), together with partner proteins, XRCC4 and XLF. Patients mutated in genes encoding LIG4, XLF or other NHEJ proteins DNA-PKcs and Artemis are DSB repair defective and immunodeficient, due to the requirement for NHEJ during V(D)J recombination.

Objective: We found a patient displaying microcephaly and progressive ataxia but a normal immune response. We sought to determine pathogenic mutations and to describe a molecular pathogenesis of the patient.

Methods: We performed NGS exome sequencing. We evaluated DSB repair activities and V(D)J recombination capacity of the patient cells as well as a standard blood immunological characterisation.

Results: We identified causal mutations in the *XRCC4* gene. The patient cells are radiosensitive and display the most severe DSB repair defect that we have encountered using patient derived cell lines. In marked contrast, a V(D)J recombination plasmid assay revealed that the patient cells did not display the junction abnormalities that are characteristic of other NHEJ-defective cell lines. The mutant protein can interact efficiently with LIG4 and functions normally in *in vitro* assays and when transiently expressed *in vivo*. However, the mutation makes the protein unstable and it undergoes proteasome-mediated degradation.

Conclusion: Our findings reveal a novel separation of impact phenotype: there is a

pronounced DSB repair defect and marked clinical neurological manifestation but no clinical immunodeficiency.

Capsule Summary

A patient with mutations in the *XRCC4* gene, encoding a DNA double-strand-break (DSB) repair factor, displayed severe radiosensitivity and neurological abnormalities but maintained normal V(D)J recombination function. Our findings suggest a separation of impact phenotype.

Key Words

DNA double strand break (DSB) repair; non-homologous end joining (NHEJ); DSB repair-deficiency; XRCC4/LIG4; immunodeficiency; microcephaly

Abbreviations

NHEJ: Non-homologous end-joining
CSR: Class switch recombination
CID/SCID: Combined or severe combined immunodeficiency
DSB: DNA double strand break
hTERT: Human telomerase reverse transcriptase
RRS: Recovery of RNA synthesis
UDS: Unscheduled DNA synthesis
RDS: Recovery of DNA synthesis
NMD: Nonsense mediated mRNA decay
PARP: poly ADP ribose polymerase
NER: Nucleotide excision repair

Introduction

DSBs arise from oxidative damage and during processes such as meiosis or V(D)J recombination. They are also the major lethal lesions generated in cellular DNA by ionizing radiation. Although DSBs do not arise at high frequency endogenously, they are a critical lesion causing cell death or carcinogenesis if misrepaired. Additionally, the development of the immune response involves the introduction of DSBs to generate the requisite genetic diversity.[1] V(D)J recombination represents one such process.[2] Class switch recombination (CSR), which involves the switching of immunoglobulin isotypes, also involves the introduction and rejoining of DSBs.[3]

NHEJ is the major DSB repair process in mammalian cells. The process is initiated by the binding of the Ku heterodimer to double-stranded DNA ends followed by the recruitment of the DNA-dependent protein kinase catalytic subunit, DNA-PKcs, generating the DNA-PK holoenzyme and activating DNA-PK activity.[4] DNA-PK has a role in end-tethering and regulates steps of end-processing. The final step of rejoining involves the recruitment of a ligation complex encompassing DNA ligase IV (LIG4), XRCC4 and XLF. LIG4 and XRCC4 interacts strongly via a tandem BRCT domain in LIG4 and a coiled coil region in XRCC4, forming a highly stable complex.[5, 6] XRCC4 is required for LIG4 stabilisation but recent findings have shown an excess of XRCC4 relative to LIG4.[7] Mutations that abolish LIG4/XRCC4 interaction prevent all NHEJ activity. XLF is a weaker binding partner. XRCC4 and XLF are structurally similar; both have a globular head domain, but the coiled coil region of XLF is shorter than that in XRCC4.[8, 9] Recent studies have reported that dimers of XRCC4 and XLF interact to form long superhelical filaments in solution, which have been proposed to promote

101 end-tethering or end-bridging downstream of the DNA-PK complex.[8, 10-12]

102 Loss of LIG4 or XRCC4 confers embryonic lethality in mice due to extensive
103 neuronal apoptosis.[13, 14] In contrast, XLF null mice are viable and do not show marked
104 immunodeficiency.[15] Mutations in *LIG4*, *DCLRE1C* (Artemis), *NHEJ1* (XLF) and
105 *PRKDC* (DNA-PKcs) in patients have been described.[16-20] LIG4 syndrome, which is
106 caused by hypomorphic mutations in *LIG4*, is characterised by growth delay,
107 microcephaly, and combined or severe combined immunodeficiency (CID/SCID). LIG4
108 syndrome cell lines show radiosensitivity, diminished ability to repair DSBs and impaired
109 V(D)J recombination. XLF defective patients, some of which have null mutations,
110 display features similar to, although often more severe than LIG4 syndrome.[18] Given the
111 close interaction and requirement of XRCC4 for LIG4 stability, the expectation was that
112 XRCC4 deficiency in patients would resemble LIG4 syndrome.

113 In contrast to this expectation, an XRCC4-deficient patient, CSL16NG, whose
114 cellular defects we describe in this paper, displayed unique clinical features similar to
115 those of Cockayne Syndrome, namely progressive neuronal degeneration including the
116 onset of ataxia, but no clinical immunodeficiency. Our cellular analysis revealed that the
117 mutational changes result in substantially reduced levels of XRCC4 protein, a marked
118 defect in DSB repair but seemingly efficient V(D)J recombination. Based on comparative
119 studies with LIG4 and XLF deficient cell lines, our results reveal a separation of impact
120 phenotype where marked deficiency in radiation-induced DSB repair capacity can be
121 uncoupled from defective V(D)J recombination. Our results give novel insights into the
122 roles of XRCC4 during DSB repair.

Methods

Human studies

Patient and control samples were obtained with local ethical approvals [University of Sussex Research Ethics Committee; Nagasaki University Ethical, Legal and Social Implications (ELSI) committee; Ethics committee for human genome studies in Research Institute of Environmental Medicine, Nagoya University]. Written informed consent was obtained from the patient.

Exome sequencing and bioinformatics

Details are described in **Supplementary Methods**. Briefly, genomic DNA prepared from CSL16NG fibroblasts was enriched using the SureSelect All Exon Kit v5 (Agilent), followed by sequencing on the Illumina Hiseq 2500 sequencer. The sequence data were analysed by a standard exome pipeline. According to a recessive inheritance model, we selected genes that carried at least one novel deleterious homozygous or more than two heterozygous changes in one gene locus (**Table S1**).

Cell cultures

Human primary or hTERT immortalized fibroblasts were derived from the XRCC4 patient (CSL16NG), LIG4 patients (F07/614, 180BR, 411BR, 2303 and 495GOS), *XLF* patients (2BN and F07/402), an XP patient (XP15BR) or healthy donors (1BR.3 and 48BR). All primary fibroblasts were cultured in Dulbecco′s Modified Eagle Medium (DMEM) or Modified Eagle Medium (MEM), supplemented with 10-15 % fetal bovine serum (FBS) and 1× penicillin-streptomycin (PS). HEK293FT cells (Invitrogen) were grown in DMEM supplemented with 10 % FBS, 1× PS, 5 mM L-glutamine, 0.1 mM

147 Non-Essential Amino Acids (NEAA) and 1 mM sodium pyruvate. Human colon cancer
148 HCT116 (RCB2979) and HCT116-XRCC4 (-/-) (RCB2981) cells were provided by the
149 RIKEN BRC through the National Bio-Resource Project of the MEXT, Japan.
150
151 **Reagents and Antibodies**
152 Antibodies used were: XRCC4 (C4 and C20, Santa Cruz Biotechnology), LIG4 (D8,
153 Santa Cruz Biotechnology; Ab80514, Abcam; 12695-1-AP, Proteintech Group), p89
154 (S-19, Santa Cruz Biotechnology), XPG (8H7, Santa Cruz Biotechnology), CSB (Bio
155 Matrix Research), V5-tag (MBL), Flag-tag (MBL), Actin (Ab8227, Abcam),
156 Alpha-tubulin (Invitrogen), XLF (ab33499, Abcam; FL-299, Santa Cruz Biotechnology),
157 53BP1 (Bethyl) and gamma H2A.X (ser139, Millipore). MG132, E64D,
158 3-Methyladenine (3-MA), Epoxomicin, and Cycloheximide (CHX) (Sigma-Aldrich).
159
160 **Quantitative RT-PCR**
161 Details are as described previously.[21] Total RNA was extracted using the RNeasy Plus
162 Mini Kit (QIAGEN). The High-capacity RNA-to-cDNA kit (Applied Biosystems) was
163 used for 1st strand synthesis. Quantitative PCR was performed using the Thermal
164 Cycler Dice Real-Time system (TaKaRa Bio) with a QuantiTect SYBR Green PCR Kit
165 (QIAGEN). For each sample, the relative mRNA expression levels were normalized
166 using the *HPRT1* gene. Error bars represent the S.D. of means of triplicate experiments.
167
168 **Lentivirus experiments**
169 Details are as described previously.[22] Recombinant lentivirus particles expressing
170 *XRCC4* and its mutants were produced. Human *XRCC4* cDNA was cloned in frame

with a C-terminal V5-tag in the *pLenti6.3*-V5-D-TOPO vector to generate *pLenti6.3-XRCC4*-V5 plasmid. The truncation mutant (XRCC4-Del), the frameshift mutant (XRCC4-Fs), and the single amino-acid substitution mutant (XRCC4-W43R) were generated from *pLenti6.3-XRCC4*-V5 by site-directed PCR mutagenesis. Sequences of the mutant plasmids were confirmed by Sanger sequencing (**Figure S1**). 48 hours after lentivirus infection, 10 μg/ml of blasticidin (Sigma-Aldrich) was added to the medium for selection of XRCC4 stably expressing cells.

Ionizing irradiation and γH2AX foci assay

Cells were seeded in 3 cm dishes or in 96-well plates (BD Falcon) and 3Gy γ-ray irradiated using a ^{137}Cs γ-ray source at a dose rate of 0.017 Gy s^{-1}, then further cultured for indicated time periods. Cells were fixed with 4 % formaldehyde and permeabilized with 0.2 % TritonX-100, followed by staining with DAPI and γH2AX antibody. Image acquisition and analysis were performed using the Cellomics ArrayScan VTI (Thermo Scientific). The average number of separate γH2AX foci was assessed on at least 300 cells.

NHEJ-, V(D)J- and CSR assays

The assays were performed as previously described.[23, 24] For NHEJ-assay, 1 μg PDVG94 plasmid, digested with *Eco*RV and *Eco*47III (Promega) to create blunt ends with 6 bp repeats, were transiently transfected into fibroblast cells using Turbofect (Fermentas). 48 h after transfection, cells were harvested and DNA extracted using DNeasy blood and tissue kit (QIAGEN). The recombined junctions were PCR amplified with primers FM30 and DAR5[23] and the PCR product was gel purified using Qiaquick

gel extraction kit (QIAGEN), cloned into pGEM-T vectors and sequenced (Macrogen). The V(D)J-assay was performed as the NHEJ-assay except that in total 1.5 μg of PDVG93 circular plasmid, RAG1 and RAG2 plasmids were transiently transfected into fibroblast cells and the coding junctions were amplified by a nested PCR using the primers NV05F (5'-CTATAGGGGAATTGTGAGCGGATAACDG-3'), DG147 and DG89, FM30.[23] Switch recombination junctions were PCR amplified, cloned, sequenced and analysed as described previously.[25, 26]

Protein purification

Detailed protein purification procedures and buffer conditions are as described previously.[21, 27] Briefly, HEK293FT cells were co-transfected with the *pLenti6.3-LIG4*-His and *pLenti6.3*-Flag-*XRCC4*, or its mutants. Cell lysates were incubated with anti-Flag M2 beads (Sigma-Aldrich) for 4 hours at 4 °C. After extensive washing of the beads, the Flag-tagged wild type (WT) or mutant XRCC4 in complex with LIG4 was eluted with Flag-peptide. The eluted complexes were dialyzed, concentrated and stored at -80°C. For expression and purification of GST-XLF protein, *E.coli* BL21 (DE3) cells were transformed with *pGEX6*-GST-*XLF* plasmid. The GST-XLF protein was induced with IPTG. The cells were harvested, lysed and cleared lysate was loaded onto a GSTrap HP column (GE Healthcare). After washing, the GST-XLF protein was eluted by reduced L-glutathione (Wako). The eluted proteins were dialyzed, concentrated and stored at -80°C.

***In vitro* DSB ligation assay**

A 934 bp Cy5-labeled double strand DNA fragment was PCR amplified from pEGFP-C3 vector using a set of primers (Forward: 5'-Cy5-GTTTCGCCACCTCTGACTTGAGCG-3'; Reverse: 5'-GAACTTCAGGGTCAGCTTGCCGTAG-3'). The DNA fragment was digested with *Nco*I (TaKaRa). A 545 bp fragment (Cy5 labeled at the 5' blunt-end and a 3'-overhang end) and a 255 bp fragment (with 4 bp overhangs at each end) were purified. The complexes were incubated for 30 min at 37 °C in a 30 μl reaction mixture (66 mM Tris-HCl pH7.5, 5 mM $MgCl_2$, 1 mM DTT, 1 mM ATP) with 50 ng of DNA substrates (the Cy5-labeled 545 bp fragment: the unlabeled 255 bp fragment = 2: 3). Reaction mixtures were pre-incubated for 10 min on ice with GST-XLF, and then LIG4-XRCC4 complex was added at 37 °C for 15 min. The reactions were terminated by adding 1.5 μl of 10 % SDS, followed by purification with QIAquick PCR Purification kit (QIAGEN). 30 μl of the eluted DNA was mixed with 10× loading buffer, incubated at 65 °C for 5 min and cooled on ice rapidly. 15 μl of the DNA was run on 1 % agarose gel and analyzed by the Typhoon imager (GE Healthcare).

Analysis of protein stability

HEK293FT cells were transiently transfected with XRCC4 or its mutant plasmids. Cells were treated with CHX (100 μg/ml) combined with MG132 (20 μM), E64D (20 μM), Epoxomicin (1 μM) or 3-MA (10 mM). Cells were harvested at the indicated time points. Whole cell lysate was analysed by Western blotting using anti-V5 antibody.

Immunoprecipitation

Immunoprecipitation of ectopically expressed WT or mutant XRCC4 proteins in

CSL16NG cells was performed on cell extracts using anti-V5 agarose (MBL). Immunoprecipitates were washed five times with lysis buffer containing 0.15 or 1 M NaCl, then eluted using V5-peptide (2 mM, MBL). The eluted proteins were separated on 5-20 % gradient SDS-PAGE gels, blotted onto PVDF membranes and analyzed by Western blotting.

Confocal Fluorescence Microscopy

Cells were washed once with PBS (Wako) and fixed with Fix buffer [300 mM sucrose, 2 % (v/v) formaldehyde, and 0.2 % (v/v) Triton X-100 in PBS]. After a brief washing in PBS, cells were blocked with 10 % FBS in PBS for 30 min and then incubated for 1 h with the anti-V5-tag, anti-γH2AX, anti-LIG4 or anti-XRCC4 antibodies at appropriate dilution. The cells were then washed three times with PBST (0.05 % Tween-20) and incubated with Alexa fluor488-conjugated secondary antibody at a dilution of 1:500 for 1 h. To visualize nuclei, the cells were incubated with DAPI (10 ng/mL) for 15 min. Cells were then washed and mounted, and examined on a LSM 700 laser scanning confocal microscope (Carl Zeiss). Images were taken with the 40× oil immersion objective lens under identical imaging settings.

Survival analysis

Fibroblasts were irradiated using a ^{137}Cs γ-ray source at a dose rate of 0.09 Gy s^{-1}. Radiosensitivity was assessed by colony survival analysis. Cells were trypsinised, irradiated and plated onto feeder cells prepared 24 h earlier and left to form colonies for three weeks. For XRCC4 complementation experiments, normal (48BR), CSL16NG and CSL16NG-derived fibroblasts expressing WT XRCC4 were seeded in 96-well

plates (BD Falcon). After γ-ray irradiation, cells are incubated for a further 24 hours. Sensitivity to IR was measured by recovery of DNA synthesis (RDS) analysis as described in supplementary methods (RRS, UDS and RDS assays).

Results

Patient CSL16NG has compound heterozygous mutations in *XRCC4*

Patient CSL16NG, the first daughter of non-consanguineous Caucasian parents, had significant intrauterine growth failure and microcephaly at birth. She showed slow growth, delayed motor development and dysmorphic features. Her stature, developmental delay, deep-set eyes and other features resembled those of Cockayne syndrome (CS). However, she had no history of photosensitivity and relatively slow progression of symptoms. She developed progressive ataxia. At 19 years, she was diagnosed with a low-grade thalamic glioma, which was not removed. She has hyperopia, diabetes mellitus, hypothyroidism, moderate hearing loss and slurred speech, although her understanding remains good. Her neurology has been described previously (Patient 3 in[28]). She has no significant infectious history and no obvious signs of abnormal immune response. Detailed routine blood immunological peripheral blood tests did not reveal any abnormality. Blood cell counts including peripheral blood lymphocyte sub-type numbers, immunoglobulin IgM, IgG and IgA levels were normal. Autoantibodies were negative and specific vaccine antigen antibody responses were present (**Table S2**). She is currently 23 years old (Her weight is 41.4 kg (<<3rd centile), head circumference 42.5 cm (<<3rd centile) (**Figure 1A**).

As a diagnosis of CS was considered, cellular tests for abnormal responses to UV light were carried out on a fibroblast culture established from a skin biopsy, but no abnormality typical of CS cells was observed (**Figures S2A-C**). Heterozygous mutations in two CS-related genes (*ERCC6/CSB* and *ERCC5/XPG*) were identified but both alleles were inherited from the asymptomatic father. Both proteins were expressed at normal levels (**Figures S2D and S2E**). Whole exome sequencing was carried out and

of the five potentially pathogenic candidate genes identified (details are described in **Supplemental Method; Tables S1**) *XRCC4* was the strongest. One mutation (c.C673T, p.R225*) introduced a premature stop codon; the second mutation (c.G760del, p.D254fs*68) was a frameshift (**Figure S3A**, confirmed by Sanger gDNA sequencing), which predicted the expression of a protein with an aberrant C-terminal 68 amino acids (aa), resulting in a 322 aa protein (normal full-length protein has 334 aa).

Allele-specific quantitative RT-PCR (qRT-PCR) using primers that selectively amplify the wild type (WT) or the mutant *XRCC4* cDNAs (**Figure S3B** and in **Table S3**) revealed extremely low expression of the p.R225* allele, consistent with strong nonsense mediated mRNA decay (NMD) caused by the premature stop codon (**Figure S3C**, middle panel; **Figure S3D**, left panel). The other allele encompassing the p.D254fs*68 frameshift mutation (designated as XRCC4-Fs hereafter) was expressed at ~30% of the total *XRCC4* expression level in normal 48BR cells (50% would be expected if fully expressed from one allele). The small decrease in the frameshift transcript level could reflect some NMD, although we note that the newly generated premature termination codon is located in the last exon, which does not normally trigger NMD. The mutational change could additionally affect the splicing efficiency or accuracy, which may also cause NMD (**Figure S3D**, middle panel; **Figure S3C**, left panel). No detectable XRCC4 was observed by immunoblotting of CSL16NG cells using a mouse anti-XRCC4 antibody with an epitope located close to the N-terminus of XRCC4 (**Figure 1B**). We could detect XRCC4 from a control fibroblast diluted ten-fold arguing that there is less than 10% of the normal level of XRCC4 in the patient cells.

XRCC4 is reported to co-stabilise LIG4.[5, 29, 30] Consistently, LIG4 was significantly reduced in CSL16NG fibroblasts assessed by immunoblotting (**Figure 1B,**

1C). The level of LIG4 appeared to vary depending on conditions and antibody (see **Figure 1B**, 2nd and 3rd panel). When compared with the *LIG4*-null cell line N114P2 (LIG4-/-), a band of LIG4 was clearly visible (**Figure 1C**) and, from the results of many experiments, we estimate a residual level of between 5 and 15% of normal. We also analysed XRCC4 expression by immunofluorescence (IF), which revealed a low signal in CSL16NG cells detectable in both the cytoplasm and nucleus (**Figure 1D**).

CSL16NG cells are radiosensitive and DSB repair defective.

CSL16NG primary fibroblasts showed marked radiosensitivity relative to control cells (**Figure 2A and Figure S4**) and reduced recovery of replication after radiation exposure **(Figure 2B)**. Further, CSL16NG cells showed diminished DSB repair capacity, assessed by enumerating γH2AX foci (**Figure 2C**, compare red and white bars). In order to confirm that these defects are attributable to the mutation in XRCC4, we analysed the ability of WT XRCC4 to correct the defect in CSL16NG cells. When lentivirus expressing *XRCC4*-Wt cDNA was used to infect CS16LNG cells, both the ability to synthesise DNA after irradiation (**Figure 2B**) and the repair of DSBs (**Figure 2C**, green bars) were restored to normal levels.

CSL16NG cells are defective in a plasmid DSB rejoining assay

We next examined the fidelity of repair in CSL16NG cells using an NHEJ end-joining assay that involved transfection of CSL16NG cells and control cells with linearised blunt end plasmids encompassing a 6 bp identical repeat at both DNA ends.[23] Whereas the junctions from control cells were preferentially repaired by direct end-joining, this type of repair was nearly absent in CSL16NG cells (2 % vs 72 % in control, **Table 1**).

342 Instead, the repair of CSL16NG cells was mediated by the usage of 6 bp
343 microhomology (78 % vs 8 % in controls) at the junctions, consistent with the loss of
344 efficient NHEJ in CSL16NG cells. A similar skewed repair pattern has previously been
345 observed in XLF-deficient cells.[24] These findings demonstrate a marked impact of the
346 mutation on the fidelity of DSB repair.
347
348 **CSL16NG cells carry out V(D)J recombination with enhanced fidelity compared to**
349 **control cells**
350 Defects in NHEJ are usually associated with immunodeficiency. Surprisingly,
351 CSL16NG has no history of chronic infections, and clinical analysis verified a normal
352 immune response (see above). To assess the capacity of CSL16NG cells to carry out
353 V(D)J recombination, we co-transfected CSL16NG cells with RAG1/2 expressing
354 plasmids together with a V(D)J substrate and assessed the fidelity of recombination.[23]
355 Strikingly, in contrast to the NHEJ assay, most coding junctions were accurately
356 rejoined with little use of microhomology or deletion formation (**Table 2**). This novel
357 V(D)J recombination phenotype contrasts with the pattern obtained with cell lines
358 derived from most LIG4 syndrome and XLF-deficient patients, where coding junctions
359 are characterized by increased deletions and microhomology usage.[16, 18, 23, 31]
360
361 **CSL16NG cells show altered repair pattern during class switch recombination**
362 To assess class switch recombination (CSR), we examined peripheral blood
363 mononuclear cells (PBMC) from CSL16NG. The patient was aged 22 when tested, thus
364 we compared her CSR junctions to our previously published 154 Sμ-Sα junctions from
365 healthy adults (**Table 3, Figure S5**). Amplification of Sμ-Sα junctions from *in vivo*

switched B lymphocytes from the patient revealed a reduced frequency of junctions repaired by direct end-joining, albeit not to a significant degree (5% vs. 18% in controls, χ^2, p=0.15), and a markedly increased frequency of repair by unusually long microhomologies (≥10 bp; 36% vs. 3% in controls). The altered pattern was similar to, but less prominent than that previously observed in XLF and LIG4 deficient patients.[24, 32] Thus, although the patient has a normal level of serum IgA, the altered pattern of the CSR junctions still clearly suggests a defect in the recombination process, which relies on the classical NHEJ machinery.

Effect of XRCC4-Fs mutation on XRCC4 function

We next examined the impact of XRCC4-Fs on XRCC4 function and protein expression. We also examined two other forms of XRCC4 protein (**Figure S6A**): XRCC4-Del has a stop codon at the position of the frameshift mutation in CSL16NG, and thus lacks the C-terminal aberrant polypeptide. XRCC4-W43R, contains an amino acid substitution p.W43R previously identified in a primordial dwarfism (PD) patient.[33] Although Trp43 is conserved, there is no current evidence for causality. Following lentivirus infection as described above, we found that all forms of the protein were expressed (**Figure S6B**). Strikingly, normal DSB-repair activity was restored, not only by expression of WT XRCC4, but also by XRCC4-Fs. Further, XRCC4-Del also complemented the CSL16NG DSB repair defect whereas XRCC4-W43R showed little complementation (**Figure 2C**, purple, blue and orange bars). Lentiviral expression results in *XRCC4* overexpression. To examine DSB repair under physiological expression levels, we also used hTERT-immortalised CSL16NG cells in a plasmid based complementation assay (**Figure S7**) and measured DSBs as 53BP1 foci in cells containing the plasmid. Full

390 complementation was found using WT XRCC4 protein and substantial, although not
391 full, correction by XRCC4-Fs (**Figure S7B**). Untransfected cells in the same population
392 showed the expected DSB repair defect.
393 These findings suggest that the mutant protein can partially function in DSB
394 repair. This function likely contributes to the residual DSB repair capacity observed in
395 CSL16NG cells. We also conclude that the W43R mutation impairs XRCC4 function.
396
397 **Biochemical characterisation of the mutant XRCC4 proteins**
398 To further examine the functional capacity of XRCC4-Fs, we purified recombinant
399 XRCC4-LIG4 complexes and examined their activity *in vitro*. Flag-tagged XRCC4-Wt,
400 XRCC4-Fs, and XRCC4-Del proteins were co-expressed with WT His-tagged LIG4 in
401 HEK293FT cells and co-purified by affinity chromatography (**Figure 3A**; GST-XLF
402 was purified from *E.coli* in **Figure 3B**). XRCC4-Fs and XRCC4-Del formed complexes
403 with LIG4, demonstrating that the XRCC4 C-terminus is dispensable for complex
404 formation.
405 *In vitro* ligation assays were performed using a fluorescent-labeled double
406 strand DNA with a 3' overhang on one side and an additional smaller double strand
407 DNA substrate with the same 3' cohesive overhang on both sides (**Figure 3C**). The
408 ability of the XRCC4-Fs and XRCC4-Del mutants to support LIG4-mediated ligation
409 was indistinguishable from that of the XRCC4-Wt. Further, the activity was efficiently
410 stimulated by XLF. We conclude that the effect of these alterations on the XRCC4/LIG4
411 enzyme activity is relatively minor. This finding explains the substantial
412 complementation when the mutant proteins are exogenously expressed.
413

XRCC4-Fs is degraded by the proteasome.

Given the low levels of XRCC4-Fs observed in CSL16NG cells and its presence in the cytoplasm, we examined whether it is subject to proteolytic degradation. To assess this, we first transiently expressed WT and mutant XRCC4 in HEK293FT cells in the presence or absence of the protein synthesis inhibitor, cycloheximide (CHX). In the presence of CHX, XRCC4-Wt protein was stable up to 12 h, whereas XRCC4-Fs was significantly degraded (**Figure 4A**). Remarkably, the XRCC4-Del protein was as stable as XRCC4-W43R. Degradation of XRCC4-Fs was inhibited by addition of the proteasome inhibitors, MG-132 and epoxomicin (**Figure 4B**) but unaffected by the cysteine protease inhibitor E64D, which inhibits calpain and lysosomal proteases, or 3-Methyladenine (3-MA), an autophagy inhibitor (**Figure 4B**). Consistent with these observations, the level of endogenous XRCC4 in CSL16NG cells was significantly enhanced by incubation in MG132 (**Figure S8**). These findings strongly suggest that XRCC4-Fs is subjected to proteasome mediated degradation, which provides an explanation for the very low (indeed undetectable) level of the mutant XRCC4 protein and the low level of LIG4 in the patient cells. In view of these findings, we predicted that the enhanced expression of exogenous WT or mutant XRCC4 in CSL16NG cells would lead to increased LIG4 levels. Indeed, overexpression of WT and XRCC4 mutant proteins in CSL16NG resulted in recovery of LIG4 protein levels (**Figure 4C,** compare lanes 3-6 with lane 2), which is consistent with the ability of XRCC4-Fs to complement the CSL16NG repair defect.

Taking the complementation analyses and the biochemical data together, we conclude that the XRCC4-Fs mutant protein can efficiently complex with LIG4 and promote DSB rejoining and that a major impact of the change is greatly reduced

XRCC4-Fs stability due to proteasomal degradation.

The mutations in CSL16NG confer a separation of impact phenotype.

Despite the DSB repair defect observed in CSL16NG cells and marked developmental features, the patient had a normal immune response and the patient cells showed enhanced accuracy in an in vitro assay for V(D)J recombination, in marked contrast to other NHEJ-deficient patients. A trivial explanation might be that there is sufficient residual DSB repair activity to support V(D)J recombination but not the efficient repair of radiation induced DSBs. To gain further insight, we carried out a comparative analysis of the efficiency of DSB repair of CSL16NG cells and a range of patient-derived fibroblasts with deficiencies in other NHEJ proteins (XLF or LIG4) (**Figure 5A**). Since LIG4 is essential, LIG4 syndrome patients have hypomorphic mutations and hence a range of clinical severities, which generally correlate with the magnitude of the repair defect.[34] Importantly, most of the LIG4 Syndrome cells examined (and in total 7/8 lines previously examined by us) repaired most DSBs induced by 3 Gy IR by 72 h (**Figure 5A** and data not shown). (495GOS had more marked sensitivity. This line, however, had normal LIG4 protein expression, raising the possibility that the mutational change could exert a dominant negative phenotype). Except for patient 180BR,[35, 36] all showed some degree of immunodeficiency. Of relevance here, the *in vitro* ligation activities of 411BR and cell line 2303 have been previously estimated to be < 1%, yet both lines rejoin the DSBs induced by 3 Gy within 72h.[34, 37] 411BR has previously been shown to express normal levels of mutant LIG4[34, 37] but, significantly, 2303 expressed lower levels of LIG4 compared to CSL16NG (**Figures 5B and 5C**). Collectively, this analysis of LIG4 syndrome cell lines strongly

suggests that only a low level of residual LIG4 activity (1% or less) suffices to repair all DSBs induced by 3 Gy IR, albeit with slow kinetics, a conclusion consistent with previous findings.[38] In marked contrast, CSL16NG fibroblasts, despite harbouring 5-15 % residual LIG4 levels had a severe DSB repair defect. The magnitude of the DSB repair defect was similar to, although more severe than, that shown by XLF-defective cells. The repair defect was evident following exposure to a low dose of radiation (0.5 Gy) and, after 3 Gy IR, 25 % of the DSBs remained unrepaired even 8 days post exposure (**Figures S9A and S9B**). Indeed, this represents possibly the most severely DSB repair defective human cell line that we have encountered. In rodent cells, defects in NHEJ proteins, including XLF can lead to DSB repair by alternative NHEJ (Alt-NHEJ).[39] However, the residual DSB repair in CSL16NG cells is not inhibited by a PARP inhibitor, KU58958 (**Figure S9C**) and displays an additive repair defect following siRNA depletion of *LIG4* (**Figure S9D**) or the addition of a DNA-PK inhibitor NU7441 (**Figures S9C),** suggesting that it does not represent Alt-NHEJ but residual canonical NHEJ activity. This is consistent with current evidence that Alt-NHEJ does not function in human cells unless Ku is absent.[40, 41] We note also that CSL16NG cells expressed close to normal levels of XLF, as did the LIG4 syndrome cells examined (**Figure 5B**).

These findings show that CSL16NG has a very severe defect in repair of DSB and importantly, they suggest that the normal immune response of the patient cannot be attributed to a mild defect in DSB repair, providing evidence for a separation of function phenotype.

Discussion.

We describe a patient with mutational changes in the NHEJ protein, XRCC4. The patient described here has unexpected clinical features for an NHEJ deficiency. Our detailed cellular analysis provides evidence for a separation of impact phenotype, namely severely defective DSB repair but normal immune responses, and reveals a clinical and cellular manifestation for mutations in XRCC4 that is unexpected and distinct from those conferred by diminished LIG4 enzyme activity.

In patient CSL16NG, the major expressed allele encodes a protein with 68 aberrant C-terminal amino acids p.(D254fs*68). The mutant protein can interact with LIG4 and is largely functional for DSB repair *in vitro* and *in vivo*. The major impact of the mutational change is to promote proteasome mediated degradation of the mutant protein, so that CSL16NG cells have very low XRCC4 protein levels.

There are two remarkable findings from our results, with important implications. First, the defect in DSB repair is significantly greater than that of cells with lower levels of LIG4, and secondly, despite this defect, V(D)J recombination is proficient and the patient does not display any gross clinical or laboratory immunodeficiency to date. We will consider these findings in turn.

DSB repair defect. Despite low XRCC4 levels, there is ~5-15 % residual LIG4 localised in the nucleus. This residual activity, by comparison with LIG4 syndrome cells, is estimated to be sufficient to affect slow DSB rejoining after 3 Gy IR, yet CSL16NG cells have a dramatic DSB repair defect. These findings, therefore, strongly suggest that there must be a role for XRCC4 in DSB rejoining that is distinct from its accepted function in stabilising LIG4.

Recent studies have shown that XLF forms filaments with XRCC4 and

current models propose that these function in DNA end-stabilisation during DSB repair.[8, 10-12] This structural role for XRCC4 in forming filaments necessitates multiple XRCC4 molecules at each DNA end and is unlikely to be fulfilled by a low level of residual XRCC4 protein. The similar DSB repair defect between XLF-deficient and CSL16NG cells supports an overlapping role in DSB repair. Thus, we propose that the marked DSB repair defect in CSL16NG cells is a consequence of insufficient XRCC4 to form filaments with XLF. In contrast, low residual LIG4, of which only 1-2 molecules are likely to be required per DSB, is sufficient to allow complete DSB repair albeit with slow kinetics (**Figure S9B**). If this hypothesis is correct, our data provide the first evidence suggesting that XRCC4's role in XLF filament formation can be uncoupled from its more direct role in ligation.

DSB repair defect and normal immune response. Despite the marked DSB repair defect in CSL16NG cells and an altered repair pattern during CSR, the patient did not display any immunodeficiency, and in a cell based assay, V(D)J recombination took place with enhanced rather than reduced accuracy. Most LIG4 syndrome cells, including line 2303, displayed combined immunodeficiency or severe combined immunodeficiency, yet our comparative analysis of DSB repair showed that most LIG4 Syndrome cells had more efficient DSB repair than CSL16NG.[16] Thus the normal immune response of CSL16NG cannot be attributed solely to a mild DSB repair defect, suggesting a separation of impact phenotype.

This raises the intriguing possibility that XRCC4's role in complex with XLF in end-stabilisation may be dispensable for V(D)J recombination. XLF-deficient patients, however, do display immunodeficiency demonstrating a role for XLF in V(D)J recombination in humans.[18] There appear to be distinctions between the requirement for

synapsis/end-stabilisation during V(D)J recombination versus the repair of genotoxic DSBs. Indeed, XLF is dispensable for V(D)J recombination in mice where ATM, DNA-PK and 53BP1 have been proposed to have redundant roles, yet XLF deficient patients frequently display pronounced immunodeficiency.[42, 43] We note that the phenotype of CSL16NG cells overlaps with that of XLF-deficient mice (ie a marked DSB repair defect but proficient V(D)J recombination).[15] Additionally in mice, RAG2 has been proposed to have a role in influencing rejoining during V(D)J recombination.[44] We note also that a recent paper identified PAXX as a new XRCC4 super-family member that functions with XRCC4 and XLF in NHEJ.[45] It is possible that there could be redundancy between PAXX and XRCC4 during V(D)J recombination but not during the repair of genotoxic DSBs. Further work is required to gain insight into the mechanism underlying these intriguing findings.

An additional novel phenotype of CSL16NG cells is that all the junctions formed in the V(D)J recombination assay involved high fidelity joining of the coding ends. This phenotype contrasts strongly with the lack of direct rejoining of DNA ends in the NHEJ plasmid assay and the CSR junction analysis, and further supports a separation of function phenotype. The basis for the difference from control cells in the V(D)J recombination assay, where small deletions/insertions can arise is unclear. However the accurate rejoining contrasts to other NHEJ deficient lines, which are characterised by large deletions and microhomology usage. Although the lack of junctional diversity seen in this fibroblast based assay might predict a diminished repertoire of T- and B- cells, it is possible that the assay does not fully reflect the *in vivo* process due to differences between fibroblasts and lymphocytes (e.g. T-cells express tdT).

Using CSL16NG fibroblasts and the assays established here, we also examined the impact of W43R, a previously described XRCC4 mutational change observed in a patient with primordial dwarfism.[33] We provide evidence that W43R is a pathological mutational change, supporting the notion that homozygous expression of XRCC4-W43R underlies the primordial dwarfism observed in the patient.

Several recent studies have also described patients with mutations in XRCC4.[46-49] Strikingly, all patients displayed microcephaly and growth delay but no overt immunodeficiency (although detailed examination of V(D)J recombination ability was not investigated in these patients). This strengthens our proposal that XRCC4 deficiency confers a separation of impact phenotype (impacting upon the repair of genotoxic DSBs but not the repair of DSBs induced during V(D)J recombination), demonstrating that this is not a finding specific to our patient. The severe DSB repair defect in CSL16NG cells also provides a potential explanation for the marked neurological phenotype observed in the patient. An unusual feature for NHEJ deficiency was the development of progressive ataxia in the patient and it is tempting to speculate that this is a consequence of persisting unrepaired DSBs. Intriguingly, a progressive neurological phenotype involving unsteady gait was recently observed in two XRCC4-deficient siblings, who similarly had no detectable residual XRCC4 protein.[49] This supports the notion that progressive ataxia could be a consequence of marked XRCC4 deficiency.

The prediction of our working model is that mutations in *XRCC4* that result in low expression of a protein capable of interacting with LIG4 will confer marked neurological deficits without associated immune deficiency. Given the striking resemblance of patient CSL16NG, when a young child, to CS patients, *XRCC4* should be considered a candidate for potential causal mutations in further patients with similar

features, including further CS-like patients with normal transcription-coupled nucleotide excision repair.

In summary, we describe a patient with mutations in *XRCC4*. The patient had marked neurological abnormalities with progressive ataxia. Our biochemical and cellular analysis provides evidence that the mutational changes in this patient confer a separation of impact phenotype with a severe defect in DSB repair but no marked defect in V(D)J recombination. Recent papers have described additional XRCC4-deficient patients with a normal immune response.[33, 46-49] As a working model, we propose that this could arise from a separation of XRCC4 function in stabilising LIG4 versus its role in forming filaments with XLF. We propose that XRCC4 is required for all DSB rejoining since LIG4 is unstable in the absence of XRCC4. However, only a low-level of protein suffices to provide sufficient LIG4 to effect slow rejoining. In contrast, XRCC4's role in filament formation with XLF is essential for efficient rejoining of genotoxic DSBs but appears to be dispensable during V(D)J recombination in human cells, possibly due to redundancy with other proteins that can promote synapsis.

Acknowledgements

We are grateful to Elena Korneeva for technical assistance, Dik van Gent and Jean-Pierre Villartay for cell lines from patients, Hironori Niki for general discussions, and to the patient's mother for much helpful clinical information.

This work was supported by a foreign researcher grant from the Japan Society for the Promotion of Science (JSPS) (P14093) to C.G.; a grant for Research for overcoming intractable diseases (H26-general-046) from The Ministry of Health Labour and Welfare of Japan, KAKENHI Grants-in-Aid for Scientific Research (B) (26291005) from JSPS, KAKENHI Grants-in-Aid for Scientific Research (A) (Overseas Academic Research) (15H02654) from JSPS and a science research grant from the Uehara Memorial Foundation to T.O; KAKENHI Grants-in-Aid for Young Scientists (A) (15H05333) from JSPS, a research grant from the Uehara Memorial Foundation, a medical research grant from Daiichi-Sankyo Foundation of Life Science and a medical research grant from Takeda Science Foundation and Special Coordination Funds for Promoting Science and Technology from the Japan Science and Technology Agency (JST) to Y.Nakazawa; the Swedish Research Council and the European Research Council (242551-ImmunoSwitch) to Q.P-H.

References

1. Gellert M. V(D)J recombination: RAG proteins, repair factors, and regulation. Annu Rev Biochem 2002; 71:101-32.
2. Alt FW, Zhang Y, Meng FL, Guo C, Schwer B. Mechanisms of programmed DNA lesions and genomic instability in the immune system. Cell 2013; 152:417-29.

3. Boboila C, Alt FW, Schwer B. Classical and alternative end-joining pathways for repair of lymphocyte-specific and general DNA double-strand breaks. Advances in immunology 2012; 116:1-49.
4. Radhakrishnan SK, Jette N, Lees-Miller SP. Non-homologous end joining: emerging themes and unanswered questions. DNA Repair (Amst) 2014; 17:2-8.
5. Critchlow SE, Bowater RP, Jackson SP. Mammalian DNA double-strand break repair protein XRCC4 interacts with DNA ligase IV. Current Biology 1997; 7:588-98.
6. Grawunder U, Zimmer D, Fugmann S, Schwarz K, Lieber MR. DNA ligase IV is essential for V(D)J recombination and DNA double-strand break repair in human precursor lymphocytes. Molecular Cell 1998; 2:477-84.
7. Mani RS, Yu Y, Fang S, Lu M, Fanta M, Zolner AE, et al. Dual modes of interaction between XRCC4 and polynucleotide kinase/phosphatase: implications for nonhomologous end joining. J Biol Chem 2010; 285:37619-29.
8. Hammel M, Rey M, Yu Y, Mani RS, Classen S, Liu M, et al. XRCC4 protein interactions with XRCC4-like factor (XLF) create an extended grooved scaffold for DNA ligation and double strand break repair. The Journal of biological chemistry 2011; 286:32638-50.
9. Williams GJ, Hammel M, Radhakrishnan SK, Ramsden D, Lees-Miller SP, Tainer JA. Structural insights into NHEJ: building up an integrated picture of the dynamic DSB repair super complex, one component and interaction at a time. DNA Repair (Amst) 2014; 17:110-20.
10. Mahaney BL, Hammel M, Meek K, Tainer JA, Lees-Miller SP. XRCC4 and XLF form long helical protein filaments suitable for DNA end protection and alignment to facilitate DNA double strand break repair. Biochemistry and cell biology = Biochimie et biologie cellulaire 2013; 91:31-41.
11. Andres SN, Vergnes A, Ristic D, Wyman C, Modesti M, Junop M. A human XRCC4-XLF complex bridges DNA. Nucleic Acids Res 2012;

655 40:1868-78.
656 12. Wu Q, Ochi T, Matak-Vinkovic D, Robinson CV, Chirgadze DY,
657 Blundell TL. Non-homologous end-joining partners in a helical dance:
658 structural studies of XLF-XRCC4 interactions. Biochem Soc Trans
659 2011; 39:1387-92, suppl 2 p following 92.
660 13. Barnes DE, Stamp G, Rosewell I, Denzel A, Lindahl T. Targeted
661 disruption of the gene encoding DNA ligase IV leads to lethality in
662 embryonic mice. Curr Biol 1998; 8:1395-8.
663 14. Frank KM, Sekiguchi JM, Seidl KJ, Swat W, Rathbun GA, Cheng HL,
664 et al. Late embryonic lethality and impaired V(D)J recombination in
665 mice lacking DNA ligase IV. Nature 1998; 396:173-7.
666 15. Li G, Alt FW, Cheng HL, Brush JW, Goff PH, Murphy MM, et al.
667 Lymphocyte-specific compensation for XLF/cernunnos end-joining
668 functions in V(D)J recombination. Mol Cell 2008; 31:631-40.
669 16. O'Driscoll M, Cerosaletti KM, Girard P-M, Dai Y, Stumm M, Kysela B,
670 et al. DNA Ligase IV mutations identified in patients exhibiting
671 development delay and immunodeficiency. Mol Cell 2001; 8:1175-85.
672 17. Woodbine L, Neal JA, Sasi NK, Shimada M, Deem K, Coleman H, et al.
673 PRKDC mutations in a SCID patient with profound neurological
674 abnormalities. J Clin Invest 2013; 123:2969-80.
675 18. Buck D, Malivert L, de Chasseval R, Barraud A, Fondaneche MC,
676 Sanal O, et al. Cernunnos, a novel nonhomologous end-joining factor,
677 is mutated in human immunodeficiency with microcephaly. Cell 2006;
678 124:287-99.
679 19. Murray JE, Bicknell LS, Yigit G, Duker AL, van Kogelenberg M,
680 Haghayegh S, et al. Extreme growth failure is a common presentation
681 of ligase IV deficiency. Hum Mutat 2014; 35:76-85.
682 20. Woodbine L, Gennery AR, Jeggo PA. The clinical impact of deficiency
683 in DNA non-homologous end-joining. DNA Repair (Amst) 2014;
684 16C:84-96.
685 21. Kashiyama K, Nakazawa Y, Pilz DT, Guo C, Shimada M, Sasaki K, et
686 al. Malfunction of nuclease ERCC1-XPF results in diverse clinical
687 manifestations and causes Cockayne syndrome, xeroderma

688 pigmentosum, and Fanconi anemia. Am J Hum Genet 2013; 92:807-19.
689 22. Jia N, Nakazawa Y, Guo C, Shimada M, Sethi M, Takahashi Y, et al. A
690 rapid, comprehensive system for assaying DNA repair activity and
691 cytotoxic effects of DNA-damaging reagents. Nat Protoc 2015;
692 10:12-24.
693 23. Verkaik NS, Esveldt-van Lange RE, van Heemst D, Bruggenwirth HT,
694 Hoeijmakers JH, Zdzienicka MZ, et al. Different types of V(D)J
695 recombination and end-joining defects in DNA double-strand break
696 repair mutant mammalian cells. Eur J Immunol 2002; 32:701-9.
697 24. Du L, Peng R, Bjorkman A, Filipe de Miranda N, Rosner C, Kotnis A,
698 et al. Cernunnos influences human immunoglobulin class switch
699 recombination and may be associated with B cell lymphomagenesis. J
700 Exp Med 2012; 209:291-305.
701 25. Stavnezer J, Bjorkman A, Du L, Cagigi A, Pan-Hammarstrom Q.
702 Mapping of switch recombination junctions, a tool for studying DNA
703 repair pathways during immunoglobulin class switching. Adv
704 Immunol 2010; 108:45-109.
705 26. Pan Q, Petit-Frere C, Dai S, Huang P, Morton HC, Brandtzaeg P, et al.
706 Regulation of switching and production of IgA in human B cells in
707 donors with duplicated alpha1 genes. Eur J Immunol 2001;
708 31:3622-30.
709 27. Riballo E, Woodbine L, Stiff T, Walker SA, Goodarzi AA, Jeggo PA.
710 XLF-Cernunnos promotes DNA ligase IV-XRCC4 re-adenylation
711 following ligation. Nucleic Acids Res 2009; 37:482-92.
712 28. Neilan EG, Delgado MR, Donovan MA, Kim SY, Jou RL, Wu BL, et al.
713 Response of motor complications in Cockayne syndrome to
714 carbidopa-levodopa. Arch Neurol 2008; 65:1117-21.
715 29. Wu PY, Frit P, Meesala S, Dauvillier S, Modesti M, Andres SN, et al.
716 Structural and functional interaction between the human DNA repair
717 proteins DNA ligase IV and XRCC4. Molecular and cellular biology
718 2009; 29:3163-72.
719 30. Modesti M, Junop MS, Ghirlando R, van de Rakt M, Gellert M, Yang W,
720 et al. Tetramerization and DNA ligase IV interaction of the DNA

721 double-strand break repair protein XRCC4 are mutually exclusive. J
722 Mol Biol 2003; 334:215-28.
723 31. Dai Y, Kysela B, Hanakahi LA, Manolis K, Riballo E, Stumm M, et al.
724 Nonhomologous end joining and V(D)J recombination require an
725 additional factor. Proc Natl Acad Sci U S A 2003; 100:2462-7.
726 32. Pan-Hammarstrom Q, Jones AM, Lahdesmaki A, Zhou W, Gatti RA,
727 Hammarstrom L, et al. Impact of DNA ligase IV on nonhomologous
728 end joining pathways during class switch recombination in human
729 cells. J Exp Med 2005; 201:189-94.
730 33. Shaheen R, Faqeih E, Ansari S, Abdel-Salam G, Al-Hassnan ZN,
731 Al-Shidi T, et al. Genomic analysis of primordial dwarfism reveals
732 novel disease genes. Genome Res 2014; 24:291-9.
733 34. Girard PM, Kysela B, Harer CJ, Doherty AJ, Jeggo PA. Analysis of
734 DNA ligase IV mutations found in LIG4 syndrome patients: the impact
735 of two linked polymorphisms. Hum Mol Genet 2004; 13:2369-76.
736 35. Riballo E, Critchlow SE, Teo SH, Doherty AJ, Priestley A, Broughton B,
737 et al. Identification of a defect in DNA ligase IV in a radiosensitive
738 leukaemia patient. Curr Biol 1999; 9:699-702.
739 36. Riballo E, Doherty AJ, Dai Y, Stiff T, Oettinger MA, Jeggo PA, et al.
740 Cellular and biochemical impact of a mutation in DNA ligase IV
741 conferring clinical radiosensitivity. J Biol Chem 2001; 276:31124-32.
742 37. O'Driscoll M, Cerosaletti KM, Girard PM, Dai Y, Stumm M, Kysela B,
743 et al. DNA ligase IV mutations identified in patients exhibiting
744 developmental delay and immunodeficiency. Mol Cell 2001; 8:1175-85.
745 38. Windhofer F, Wu W, Iliakis G. Low levels of DNA ligases III and IV
746 sufficient for effective NHEJ. J Cell Physiol 2007; 213:475-83.
747 39. Deriano L, Roth DB. Modernizing the nonhomologous end-joining
748 repertoire: alternative and classical NHEJ share the stage. Annu Rev
749 Genet 2013; 47:433-55.
750 40. Ghezraoui H, Piganeau M, Renouf B, Renaud JB, Sallmyr A, Ruis B, et
751 al. Chromosomal translocations in human cells are generated by
752 canonical nonhomologous end-joining. Mol Cell 2014; 55:829-42.
753 41. Oh S, Harvey A, Zimbric J, Wang Y, Nguyen T, Jackson PJ, et al. DNA

754 ligase III and DNA ligase IV carry out genetically distinct forms of end
755 joining in human somatic cells. DNA Repair (Amst) 2014; 21:97-110.
756 42. Zha S, Guo C, Boboila C, Oksenych V, Cheng HL, Zhang Y, et al. ATM
757 damage response and XLF repair factor are functionally redundant in
758 joining DNA breaks. Nature 2011; 469:250-4.
759 43. Liu S, Opiyo SO, Manthey K, Glanzer JG, Ashley AK, Amerin C, et al.
760 Distinct roles for DNA-PK, ATM and ATR in RPA phosphorylation and
761 checkpoint activation in response to replication stress. Nucleic Acids
762 Res 2012; 40:10780-94.
763 44. Gigi V, Lewis S, Shestova O, Mijuskovic M, Deriano L, Meng W, et al.
764 RAG2 mutants alter DSB repair pathway choice in vivo and illuminate
765 the nature of 'alternative NHEJ'. Nucleic Acids Res 2014; 42:6352-64.
766 45. Ochi T, Blackford AN, Coates J, Jhujh S, Mehmood S, Tamura N, et al.
767 DNA repair. PAXX, a paralog of XRCC4 and XLF, interacts with Ku to
768 promote DNA double-strand break repair. Science 2015; 347:185-8.
769 46. Rosin N, Elcioglu NH, Beleggia F, Isguven P, Altmuller J, Thiele H, et
770 al. Mutations in XRCC4 cause primary microcephaly, short stature
771 and increased genomic instability. Hum Mol Genet 2015.
772 47. Murray JE, van der Burg M, H IJ, Carroll P, Wu Q, Ochi T, et al.
773 Mutations in the NHEJ component XRCC4 cause primordial dwarfism.
774 Am J Hum Genet 2015; 96:412-24.
775 48. de Bruin C, Mericq V, Andrew SF, van Duyvenvoorde HA, Verkaik NS,
776 Losekoot M, et al. An XRCC4 splice mutation is associated with severe
777 short stature, gonadal failure, and early-onset metabolic syndrome. J
778 Clin Endocrinol Metab 2015:jc20151098.
779 49. Bee L, Nasca A, Zanolini A, Cendron F, d'Adamo P, Costa R, et al. A
780 nonsense mutation of human XRCC4 is associated with adult-onset
781 progressive encephalocardiomyopathy. EMBO Mol Med 2015.
782 50. Frank KM, Sharpless NE, Gao Y, Sekiguchi JM, Ferguson DO, Zhu C,
783 et al. DNA ligase IV deficiency in mice leads to defective neurogenesis
784 and embryonic lethality via the p53 pathway. Mol Cell 2000;
785 5:993-1002.
786 51. Enervald E, Du L, Visnes T, Bjorkman A, Lindgren E, Wincent J, et al.

A regulatory role for the cohesin loader NIPBL in nonhomologous end joining during immunoglobulin class switch recombination. J Exp Med 2013; 210:2503-13.

52. Nakazawa Y, Yamashita S, Lehmann AR, Ogi T. A semi-automated non-radioactive system for measuring recovery of RNA synthesis and unscheduled DNA synthesis using ethynyluracil derivatives. DNA Repair (Amst) 2010; 9:506-16.

53. Limsirichaikul S, Niimi A, Fawcett H, Lehmann A, Yamashita S, Ogi T. A rapid non-radioactive technique for measurement of repair synthesis in primary human fibroblasts by incorporation of ethynyl deoxyuridine (EdU). Nucleic Acids Res 2009; 37:e31.

Figure legends

Figure 1. Identification of mutations in the *XRCC4* gene in CSL16NG

(A) Clinical pictures of CSL16NG at age 1.5, 16 and 23 (with informed written consent from the patient's mother). (B) Immunoblotting of XRCC4 and LIG4 proteins in CSL16NG and HCT116-XRCC4 (-/-) cells as well as normal 48BR, 1BR.3 and HCT116 cells with alpha-tubulin as a loading control. The black solid arrows indicate the position of each protein. The dilutions indicate that the amount of XRCC4 in the patient cells is < 2% (detection limit) of normal cells. (C) Immunoblots showing the expression of LIG4 proteins in normal (48BR), patient (CSL16NG) and N114P2 (LIG4 -/-) fibroblasts. (D) Immunofluorescent staining of endogenous XRCC4 protein in normal 48BR, CSL16NG cells. Cells were fixed and immunostained with mouse anti-XRCC4 antibody (C4, Green). DAPI, DAPI staining (Blue); Merge, merged picture; Scale bar, 20 μm.

Figure 2. CSL16NG defects in DNA double strand break repair

(A) The colony-forming ability of primary CSL16NG cells was compared with that of a normal control (1BR.3) and that of a *LIG4*-defective F07/614 cells after treatment with different doses of γ-ray. The range of sensitivity displayed by another healthy individual and 20 other individuals deemed to have a normal (or close to normal) response is shown in **Figure S4**. In (A), all primary cell lines used were between 5 and 9 passages following establishment from a skin biopsy. Error bars represent S.D. obtained from triplicate experiments. (B) CSL16NG cell sensitivity to γ-ray was rescued by overexpression of the WT XRCC4 protein. Cell proliferation 24 hrs after γ-irradiation was determined by EdU incorporation and compared with that in unirradiated cells. (C) Complementation of the DSB repair defect in CSL16NG cells. CSL16NG cells stably expressing the V5-tagged WT XRCC4 or the indicated mutant XRCC4 proteins were irradiated with 3 Gy IR. DSB repair kinetics was measured as described above. In (B,C), primary cell lines used were between 16 and 20 passages following establishment from a skin biopsy. Error bars represent S.D. obtained from triplicate experiments.

Figure 3. The XRCC4-Fs-DNA ligase IV complex has normal ligase activity

(A) His-tagged LIG4 and the FLAG-tagged WT and the mutant XRCC4 proteins were expressed in HEK293FT cells. Total cell lysates were prepared and the XRCC4-DNA ligase IV complexes were purified on anti-FLAG M2 beads as described in **Materials and Methods**. Purified proteins were run on a SDS-PAGE and either stained with Coomassie brilliant blue (left panel) or immunoblotted with antibodies against LIG4 or XRCC4 as indicated (right panel). (B) GST-tagged XLF was purified from *E. coli* BL21 according to the methods described previously.[27] (C) The purified XRCC4-DNA ligase

838 IV complexes and XLF were incubated with the indicated Cy5-labeled and non-labeled
839 dsDNA substrates. Ligated products diagrammed at right of figure were identified on
840 1 % agarose gel electrophoresis by their decreased mobility.
841
842 **Figure 4. XRCC4-Fs mutant protein is unstable in cells**
843 (A) Immunoblots of the WT and mutant XRCC4 proteins with CHX (100 μg/ml). (B)
844 Effects of various chemical compounds on degradation of the XRCC4-Fs protein.
845 HEK293FT cells were transiently transfected with the XRCC4-Fs cDNA and treated
846 with cycloheximide together with proteasome inhibitors, MG132 (20 μM) or
847 epoxomicin (1 μM), protease inhibitor E64D (20 μM), or autophagy inhibitor 3-MA (10
848 mM) for the indicated period. DMSO was used as a vehicle control. (C) Overexpression
849 the WT and the mutant XRCC4 proteins restored LIG4 expression levels. V5-tagged
850 XRCC4-Wt or mutant proteins were ectopically expressed in CSL16NG cells and the
851 levels of LIG4 were analysed by immunoblotting with two different antibodies.
852
853 **Figure 5. CSL16NG cells show an exceptionally marked DSB repair defect.**
854 (A) Double strand break (DSB) repair kinetics following γ-irradiation were determined
855 in normal and various DSB-repair deficient patient cell lines. Residual DSBs were
856 measured by enumeration of the average number of γH2AX foci at each indicated time
857 point. (B) Immunoblots showing the expression of XRCC4, LIG4 and XLF proteins in
858 cells from normal individuals (1BR.3), patient (CSL16NG) as well as previously
859 reported XLF-patient (2BN) and LIG4-patients (F07/614 and 2303). (C) Diminished
860 expression of the LIG4 in CSL16NG cells were confirmed by immunofluorescent
861 staining. DAPI, DAPI (Blue). All primary fibroblasts used were between 5 and 9

862 passages following establishment from a skin biopsy. Error bars represent S.D. obtained

863 from triplicate experiments.

Table 1. Increased microhomology-dependent repair in CSL16NG ells in plasmid-based NHEJ assay[a]

Cell line	Direct end-joining	6bp MH	Deletion+MH	Deletion only	Total No. of junctions
CSL16NG	**1 (2%)***↓**	**47 (78%)***↑**	3 (5%)	9 (15%)	60
XLF$^{-/-}$[b]	**3 (4%)***↓**	**55 (81%)***↑**	10 (15%)	**0 (0%)**↓**	68
411BR LIG4d[c]	**4 (22%)***↓**	**12 (67%)***↑**	0 (0%)	2 (11%)	18
Controls[d]	105 (72%)	11 (8%)	14 (10%)	16 (11%)	146

a. Statistical calculations performed by χ^2 test. Significant changes are indicated in bold. **p*<0.05, ***p*<0.01, ****p*<0.001

b. Previously published results from XLF-deficient cell line.[24]

c. 411BR, described in.[16, 50]

d. Newly generated results merged with previously published results from control cell line.[24, 51]

Table 2. Increased fidelity of end joining at coding junctions in CSL16NG in plasmid-based VDJ-assay[a]

Cell line	Accurate end-joining	4bp MH	Deletion+MH	Deletion only	Total No. of junctions
CSL16NG	**18 (90%)***↑	**0 (0%)*↓**	**2 (10%)**↓**	**0 (0%)*↓**	20
XLF$^{-/-}$	5 (12%)	4 (10%)	**32 (78%)***↑**	**0 (0%)***↓**	41
Controls	13 (10%)	25 (20%)	57 (46%)	30 (24%)	125

a. Statistical calculations performed by χ^2 test. Significant changes are indicated in bold.

*p<0.05, **p<0.01, ***p<0.001

877 **Table 3. Characterization of Sμ-Sα junctions[a]**

Patients	Perfectly matched short homology						Total No. of S fragments
	0 bp		1-3 bp	4-6 bp	7-9 bp	≥ 10 bp	
	Direct end-joining	Small insertions					
CSL16NG (n=1)	1 (5%)	2 (9%)	4 (18%)	2 (9%)	**5 (23%)*↑**	**8 (36%)***↑**	22
LIG4d[b] (n=2)	**0 (0%)*↓**	**1 (3%)**↓**	7 (23%)	4 (13%)	4 (13%)	**14 (47%)***↑**	30
Controls[b] (n=17)	28 (18%)	39 (25%)	56 (36%)	15 (10%)	11 (7%)	5 (3%)	154

878 a. Statistical analysis was performed using χ^2 test and significant differences are
879 indicated in bold. * $p<0.05$, ** $p<0.01$, *** $p<0.001$.
880 b. Previously published junctions from *LIG4*-deficient patients and controls.[32]
881 n= Indicates number of individuals in each group.
882

Supplemental Materials

Supplemental methods

RRS, UDS and RDS assays

Detailed experimental procedures have been described previously.[22, 52, 53] Briefly, normal 48BR, CSL16NG and XPA patient-derived primary fibroblasts (XP15BR) were seeded in 96-well plates (BD Falcon). For RRS assay, cells were UV-irradiated (254 nm UVC, 12 J/cm^2) and incubated for 12 hours for RNA synthesis recovery, followed by ethynyluridine (EU) incorporation. For the UDS and RDS assays, UV- or γ-ray irradiated cells were immediately incubated with 5'-ethynyl-2'-deoxyuridine (EdU) for measuring repair synthesis. After incorporation of EdU or EU, cells were fixed, followed by Alexa Fluor 488-azide coupling and DAPI staining. Image acquisition and data processing were automated using the Cellomics ArrayScan VTI (Thermo Scientific).

Identification of the pathogenic mutations by exome sequencing

We performed exome sequencing of the patient, CSL16NG, using the Agilent SureSelect Exome Target Enrichment System (version.5 50Mbp target), followed by paired-end sequencing (101 bp/read) on the Illumina Hiseq 2500 sequencer. We obtained ~193 million reads (~ 19 Giga base pairs). Of the QC-passed initial sequencing reads, 18.4 Gbp are uniquely mapped to the human reference sequence (b37). Of the mapped sequences, 12.9 Gbp (66.33%) are further mapped to the target exon regions with a mean coverage of 89.05x. 98.8% of the target bases were read more than 2x coverage. We identified a total of 740,166 single nucleotide variants (SNVs) and 88,210 insertions and deletions (indels). To identify potential pathogenetic changes, we firstly

909 determined 'functionally significant variants', which are coding non-synonymous SNVs,
910 stopgains and stoplosses, splice-site variants, and coding indels. We identified 11,505
911 functionally significant variants. The identified variants were then filtered out to extract
912 'novel functionally significant variants'. We compared the identified variants with
913 dbSNP137, 1000 Genomes Project, and 88 in-house exome sequencing data. Variants
914 found in these databases were excluded. As a consequence of these filtering process,
915 totally 140 novel functionally significant variants were determined. Based on a
916 recessive inheritance model, we found 5 pathogenic candidate genes in the patient
917 (**Table S1**).
918

Table S1. Novel homozygous and compound heterozygous variants in the candidate genes identified by the exome sequencing of the patients CSL16NG.

Patient	Chr.	Position	Genotype	Gene	Mutation type	Nucleotide change	Amino-acid change
CSL16NG	3	184104702	Het	*CHRD*	ns	c.G2266A	p.D756N
CSL16NG	3	184103873	Het	*CHRD*	ns	c.C1858T	p.R620W
CSL16NG	**5**	**82554363**	**Het**	***XRCC4***	**fs del**	**c.760delG**	**p.D254fs**
CSL16NG	**5**	**82500668**	**Het**	***XRCC4***	**sg**	**c.673T**	**p.R225***
CSL16NG	9	35906600	Hom	*HRCT1*	fs ins	c.316_317insA	p.P106fs
CSL16NG	11	1266064	Het	*MUC5B*	ns	c.A7963G	p.I2655V
CSL16NG	11	1247871	Het	*MUC5B*	ns	c.G226T	p.V76L
CSL16NG	19	1863385	Hom	*KLF16*	ns	c.G112A	p.A38T

Abbreviations used in this table: Chr., chromosome; Position, refseq position of the variant; Genotype, Hom / homozygous, Het / heterozygous; Gene, gene symbol in which the variant is located; Mutation type, ns / nonsynonymous missense, fs del / frameshift deletion, fs ins / frameshift insertion, sg / stop gain; Nucleotide change, base change and base number resulting from the observed variant; Amino acid change, amino acid change and codon number resulting from the observed variant.

Table S2. Blood immunological tests on CSL16NG

Immunological parameter	Value	Age-related normal range
CD3	1973 cells/μl	(690-2540)
CD4	1210 cells/μl	(410-1590)
CD8	744 cells/μl	(190-1140)
CD19	615 cells/μl	(90-660)
CD16/56	1506 cells/μl	(90-590)
CD45RACD27	200 cells/μl	
TCRαβ	98%	
TCRγδ	2%	
CD27-IgM+IgD+	85%	
CD27+IgM+IgD+	5%	
CD27+IgM-IgD-	7%	
IgM	1.66 g/L	(0.71-2.30)
IgA	1.26 g/L	(0.64-2.97)
IgG	7.7 g/L	(5.8-15.4)

Table S3. Primers used for allele-specific amplification.

Primer designation	Primer sequence
XRCC4-F	5’-GTGTGAGTGCTAAGGAAGCTTTGG-3’
XRCC4-WT-R	5’-TACTCTCATCATAGACTGGATCTCG-3’
XRCC4-ter-R	5’-TACTCTCATCATAGACTGGATCTCA-3’
XRCC4-com-R	5’-GTACTCTCATCATAGACTGGATCTC-3’
XRCC4-R	5’-CTTCTGGGCTGCTGTTTCTCAGAG-3’
XRCC4-WT-F	5’-TTCAGCTGCTGTAAGTAAAG-3’
XRCC4-fs-F	5’-TTCAGCTGCTGTAAGTAAAA-3’
XRCC4-com-F	5’-CTTCAGCTGCTGTAAGTAAA-3’

Supplemental Figures

Figure S1 Construction of XRCC4 mutants

(A) Sequence validation of constructed *pLenti-6.3-XRCC4-Del* and *pLenti-6.3-XRCC4-Fs* plasmid DNA. Red arrows indicated mutation sites. (B) Sequence validation of constructed *pLenti-6.3-XRCC4-W43R* plasmid DNA.

Figure S2. CSL16NG cells display normal NER activity

(A) Recovery of RNA synthesis (RRS) and (B) unscheduled DNA synthesis (UDS) are normal in CSL16NG. Nucleotide excision repair (NER)-proficient normal 48BR and -deficient XP15BR cells were used as controls. (XP represents xeroderma pigmentosum, a human disorder caused by NER-deficiency. XP causes sensitivity to ultraviolet (UV) irradiation and not to ionising radiation). Filled bars, 12 J/m^2 of 254 nm UV-C; open bars, no UV. (C) UV-sensitivity of different cell strains was determined after different doses of UVC irradiation, and their viability measured by their ability to incorporate EdU (5 μM, 1 h incubation) 24 hours after treatment. (D) Normal expression levels of the CSB and XPG proteins in CSL16NG cells. (E) Quantitation of data in (D). N.S., no statistically significant difference. All primary cell lines used were between 16 and 20 passages following establishment from a skin biopsy.

Figure S3. Expression of the *XRCC4* pathogenic alleles in CSL16NG cells

(A) Capillary Sanger sequencing confirmed that the patient is compound heterozygous for the c.673C>T in *XRCC4* exon 6, resulting in the premature stopgain p.R225* (inherited from the mother) as well as for the c.760delG in *XRCC4* exon 7, causing the frameshift p.D254fs*68 (inherited from the father). The altered amino acids are shown

955 in red. (B) Locations of the primer sets used for the qRT-PCR experiments are depicted.
956 (C) Selective quantitative amplification of the WT and the mutational p.Arg225*
957 *XRCC4* alleles in CSL16NG, and normal 48BR cells. Allele-specific primers selectively
958 amplify the WT (c.673C) allele (XRCC4-F and XRCC4-WT-R, left panel), the
959 pathogenic mutant (c.673C>T) allele (XRCC4-F and XRCC4-ter-R, middle panel), and
960 both alleles at once (XRCC4-F and XRCC4-com-R, right panel). (D) Selective
961 quantitative amplification of the WT and the mutational p.Asp254fs*68 *XRCC4* alleles
962 in CS16LNG, and normal 48BR cells. Allele-specific primers selectively amplify the
963 WT (c.760G) (XRCC4-WT-F and XRCC4-R, left panel), the pathogenic mutant
964 (c.760del) allele (XRCC4-fs-F and XRCC4-R, middle panel), and both alleles at once
965 (XRCC4-com-F and XRCC4-R, right panel). Transcripts from the *HPRT1* gene were
966 used as a quantification control. All primary cell lines used were between 16 and 20
967 passages following establishment from a skin biopsy.
968
969 **Figure S4 Range of radiosensitivity observed in normal patients.**
970 Figure 2A shows the sensitivity of CSL16NG primary fibroblasts relative to control
971 cells. To confirm that the sensitivity of CSL16NG cells lies outside of the normal range,
972 we firstly compared the sensitivity to 1BR.3 and 48BR primary fibroblasts, both of
973 which are derived from a healthy individual. The sensitivity of 48BR cells was similar
974 to that shown by 1BR.3 cells. To assess the magnitude of sensitivity of a broader range
975 of individuals, we included the analysis of the most recent 20 primary fibroblasts lines
976 from individuals whose cells were sent to our laboratory for analysis. These individuals
977 had a range of clinical features, including aspects of immunodeficiency. We excluded all
978 cell lines where we had an identified genetic defect. Since these cell lines were from

non-healthy individuals, we excluded the two most sensitive lines, considering that they might be from individuals with minor genetic defects affecting radiosensitivity, resulting in the analysis of 90% of this patient subset, which we considered might represent the response of a 90% percentile. The figure shows the range of sensitivity displayed by these 18 cell lines. The response of 1BR.3 and 48BR lies within this range. The lower edge of this range may be slightly more sensitive than the true responses of healthy individuals since our 18 patients were individuals with health issues. CSL16NG cells were substantially outside of this normal range.

Figure S5. Increased microhomology usage at Sμ-Sα junctions from CSL16NG

(A) Schematic picture showing regions encoding IgM (Cμ) and IgA (Cα) on IGH locus. An Sμ-Sα junction created after switching from IgM to IgA is depicted below. (B) Switch fragments from either control (C369) or patient (CSL16NG) aligned with germline Sμ and Sα sequences are shown. Determination of repair pattern was performed as previously described.[25]. Repair by direct end-joining is designated by straight line, small insertion is underlined and microhomology-based end-joining is marked by a box. The positions of break points in germline S regions are indicated by ▼ or ▲.

Figure S6 Ectopic expression of the XRCC4 mutant proteins

(A) Schematic representation of human full-length XRCC4 and XRCC4 mutants used for the complementation analyses. The light blue box indicates an aberrant C-terminal 68 amino acids (aa). (B) Percentages of XRCC4 expressing cells were confirmed by immunofluorescent staining of the V5-tagged proteins.

Figure S7. *XRCC4* cDNA complements the DSB repair defect (53BP1)

(A, B) 1BR.3 normal, and CSL16NG hTERT immortalized fibroblasts were transfected with GFP-tagged full-length *XRCC4* cDNA (XRCC4-Wt) or mutant XRCC4 (XRCC4-Fs). 24 hours after transfection, cells were irradiated with 3 Gy γ-rays, and the number of 53BP1 foci in GFP-positive cells was enumerated at 0.25 and 8 hours. Substantial correction of the DSB repair defect of patient cells was observed upon expression of both WT and mutant *XRCC4* cDNA. No correction was observed after transfection of *XRCC4* cDNA into *LIG4*-defective cells. BG, background (no irradiation); Error bars, S.D. of mean of triplicate experiments. In this experiment, the green channel detected both 53BP1 + GFP-tagged XRCC4. It was possible to identify defined 53BP1 foci above the background GFP signals of transfected cells although this is difficult to convey in the images. 53BP1 foci were enumerated in untransfected (low pan nuclear GFP signal) and in transfected (high pan nuclear signal) cells. Untransfected 1BR.3 cells have a strong XRCC4 signal, some residual 53BP1 foci at 8 h post 3 Gy and little background GFP signal. Untransfected CSL16NG cells have a low XRCC4 signal, elevated 53BP1 foci compared to 1BR.3 cells. Transfected CSL16NG cells expressing WT-XRCC4 have close to a WT level of XRCC4, reduced residual 53BP1 foci and strong GFP pan nuclear staining. Transfected CSL16NG cells expressing XRCC4-Fs showed a good nuclear staining of XRCC4 as well as some cytoplasmic staining, a strong pan nuclear signal of GFP and a number of 53BP1 foci that was slightly higher than that shown in cells expressing WT-XRCC4. The enumeration of 53BP1 foci in untransfected 1BR.3 or CSL16NG cells was similar to that observed in other experiments using these cells.

Figure S8. Proteasomal degradation of the endogenous XRCC4-Fs mutant protein

(A) Normal 48BR and CSL16NG cells were treated with CHX (100 μg/ml), MG132 (20 μM), or with epoxomicin (1 μM) for 12 hours. Immunofluorescent staining was conducted using mouse anti-XRCC4 antibody (C4, Green). DAPI, DAPI staining (Blue); Merge, merged picture; Alexa 488 only, staining only with Alexa fluor 488-conjugated secondary antibody; Scale bar, 100 μm. (B) 48BR and CSL16NG cells were treated with MG132 (20 μM) for 12 hours, the total cell lysates were subjected to SDS-PAGE and Western Blotting analysis using anti-XRCC4 or anti-DNA Ligase IV antibodies.

Figure S9. CSL16NG defects in DSB repair

(A) Normal 1BR.3 and CSL16NG primary fibroblasts were irradiated with 0.5 Gy γ-ray. The average number of γH2AX foci was enumerated at the indicated times. Results represent the mean +/- S.D. of 3 experiments. (B) Normal 48BR, CSL16NG, 2BN (XLF-defective) and 2303 (LIG4 syndrome) cells were untreated or treated with 3 Gy γ-ray and incubated for 8 days to allow DSB repair. γH2AX foci were enumerated at the indicated times. Results represent the mean +/- S.D. of 3 experiments (C) Normal 48BR and CSL16NG cells were treated with 3 Gy γ-irradiation and incubated with or without the 0.5 μM PARP inhibitor (KU58958, a kind gift from AstraZeneca) or 5 mM DNA-PK inhibitor (NU7441, Stratech Scientific, UK) for the indicated times. (D) Left panel, knockdown of *LIG4* in CSL16NG hTERT cells shows an additive DSB repair defect demonstrating that there is residual NHEJ activity. "+ LigIV kd" represents

knockdown of *LIG4* prior to IR and γH2AX analysis; Right panel images show two cells (top image, DAPI; 2nd image, γH2AX; 3rd and 4th image, LIG4). The cell with a solid asterisk has undergone knockdown, the other has not. The cell with knockdown has a greater level of DSBs remaining as shown by intense γH2AX staining. The bottom image has been amplified to show enhanced intensity of staining. This image shows that even in the knocked down CSL16NG hTERT cells, there is residual detectable LIG4. Thus, the residual DSB rejoining is most likely still attributable to residual NHEJ. All primary cell lines used were between 5 and 9 passages following establishment from a skin biopsy. Error bars in panels A and B represent S.D. obtained from triplicate experiments. Where only two experiments were carried out (C and D) individual experiments have been plotted side by side.

Figure 1

Click here to download high resolution image

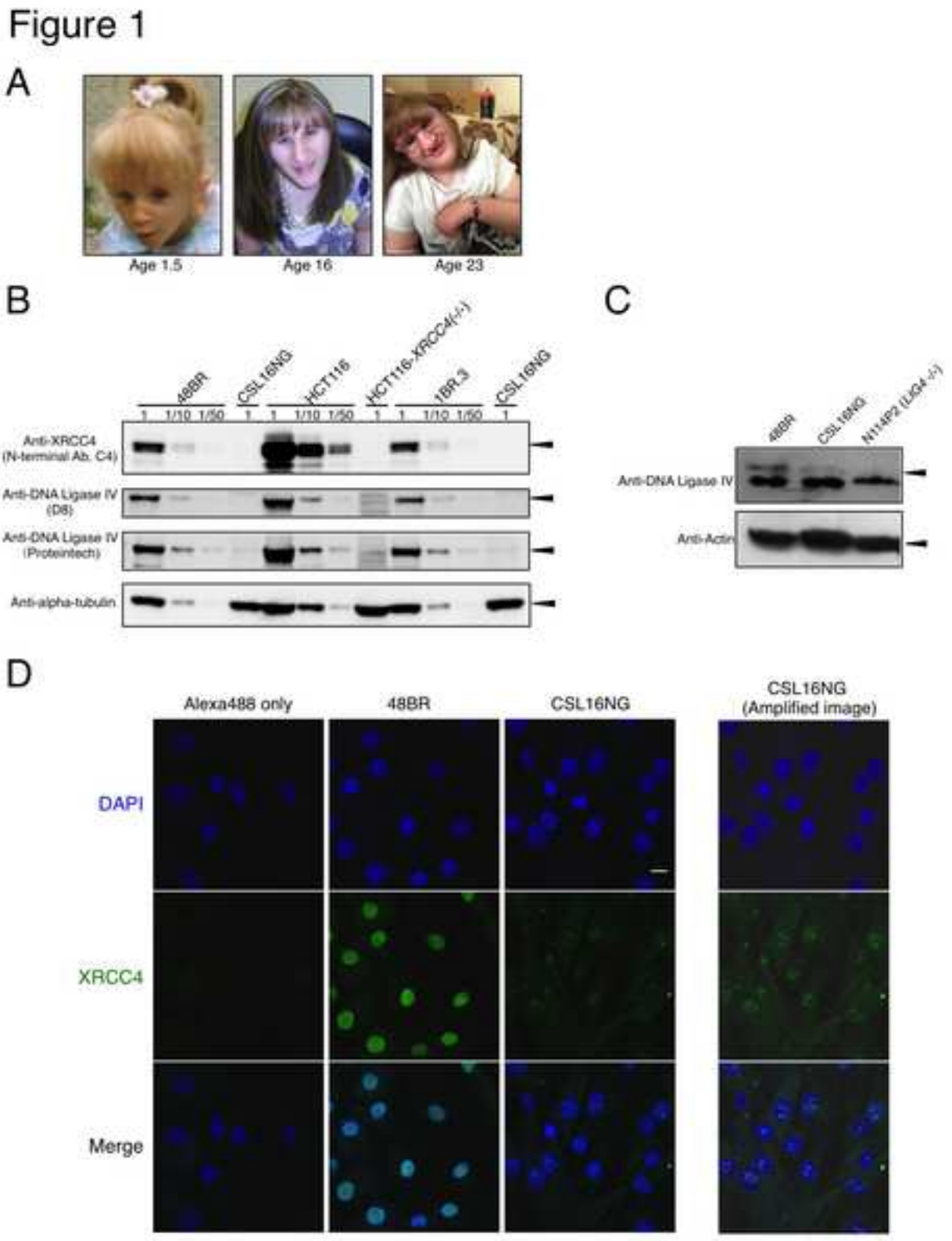

Figure 2

Click here to download high resolution image

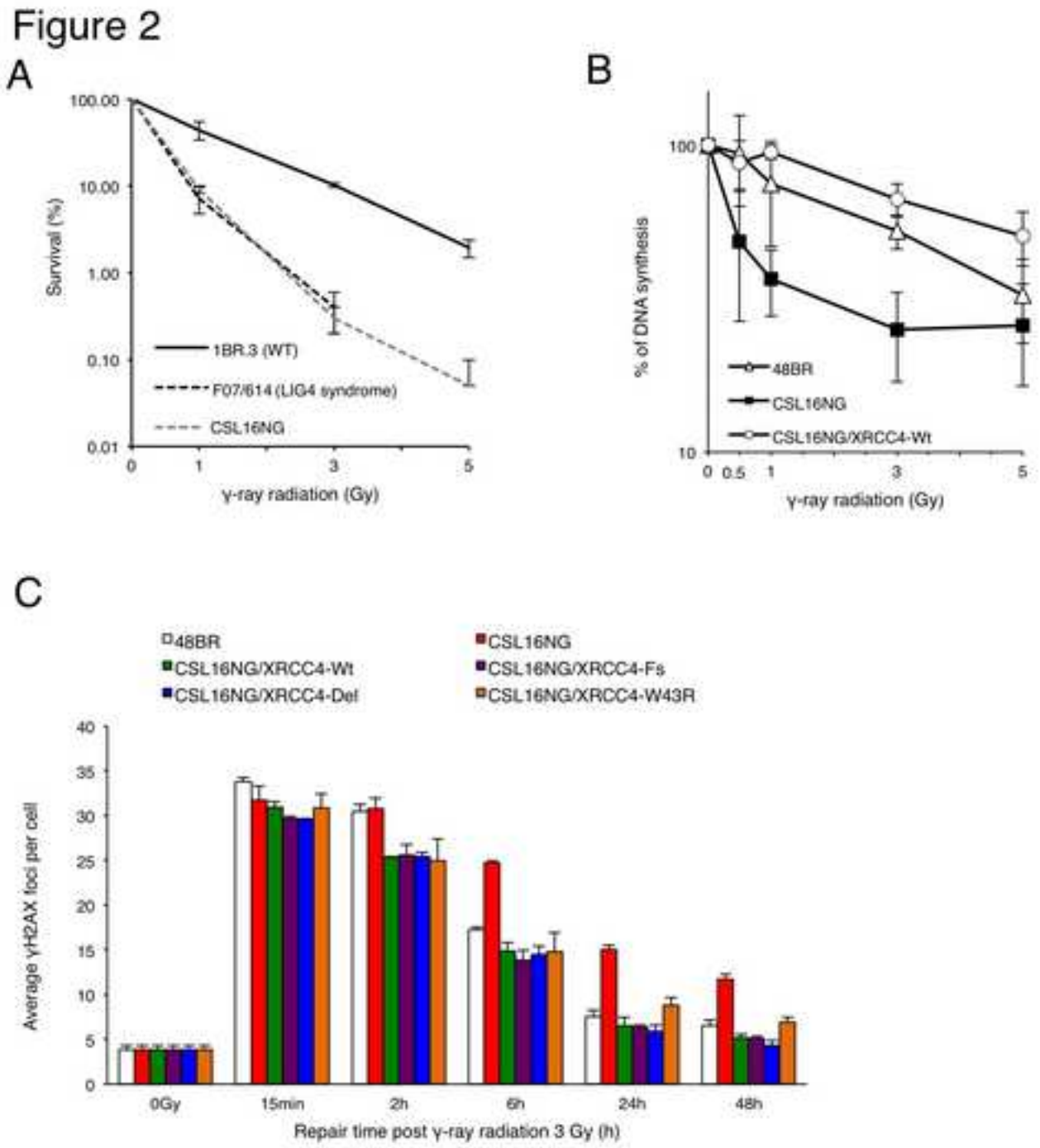

Figure 3

Click here to download high resolution image

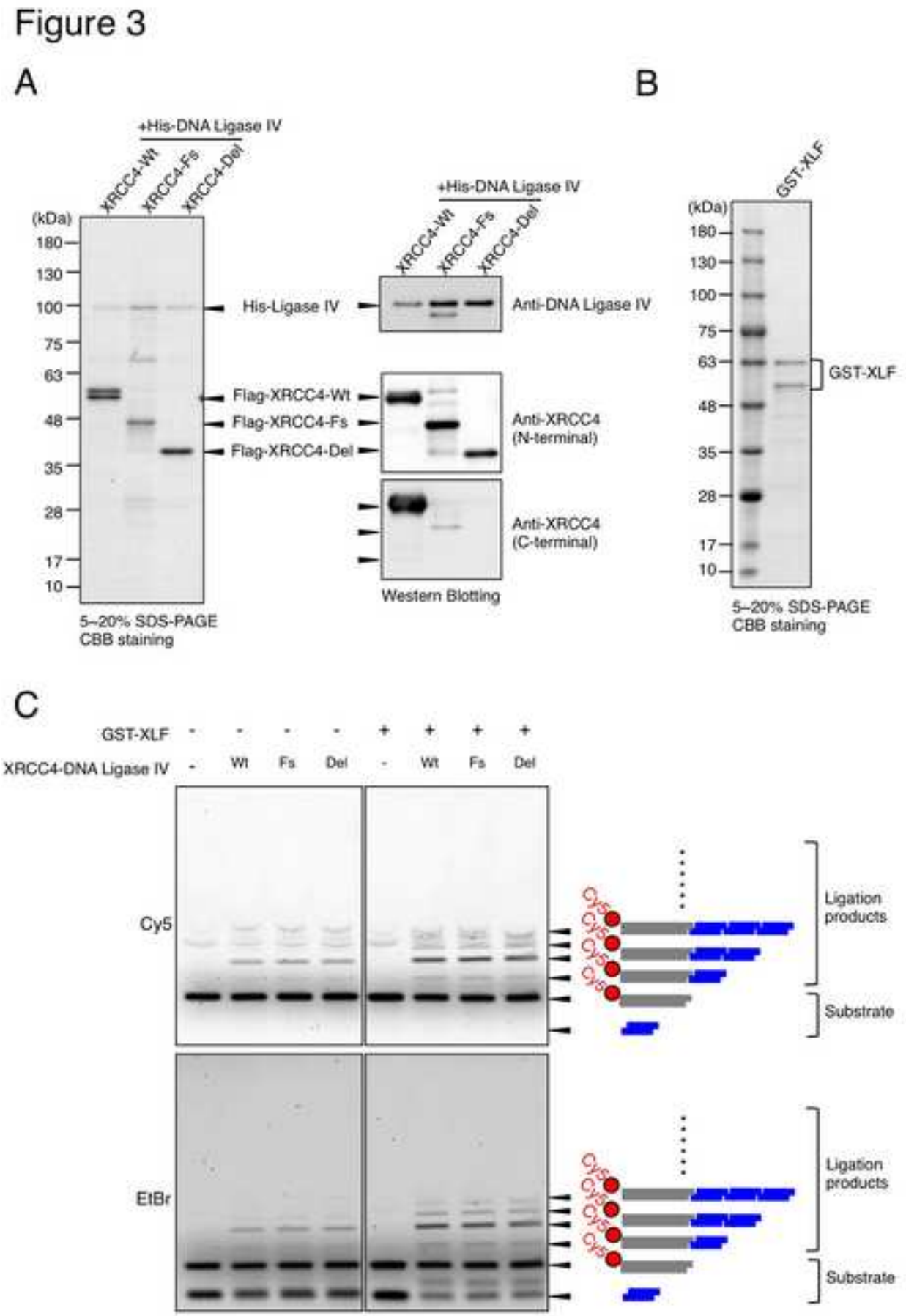

Figure 4

Click here to download high resolution image

Figure 4

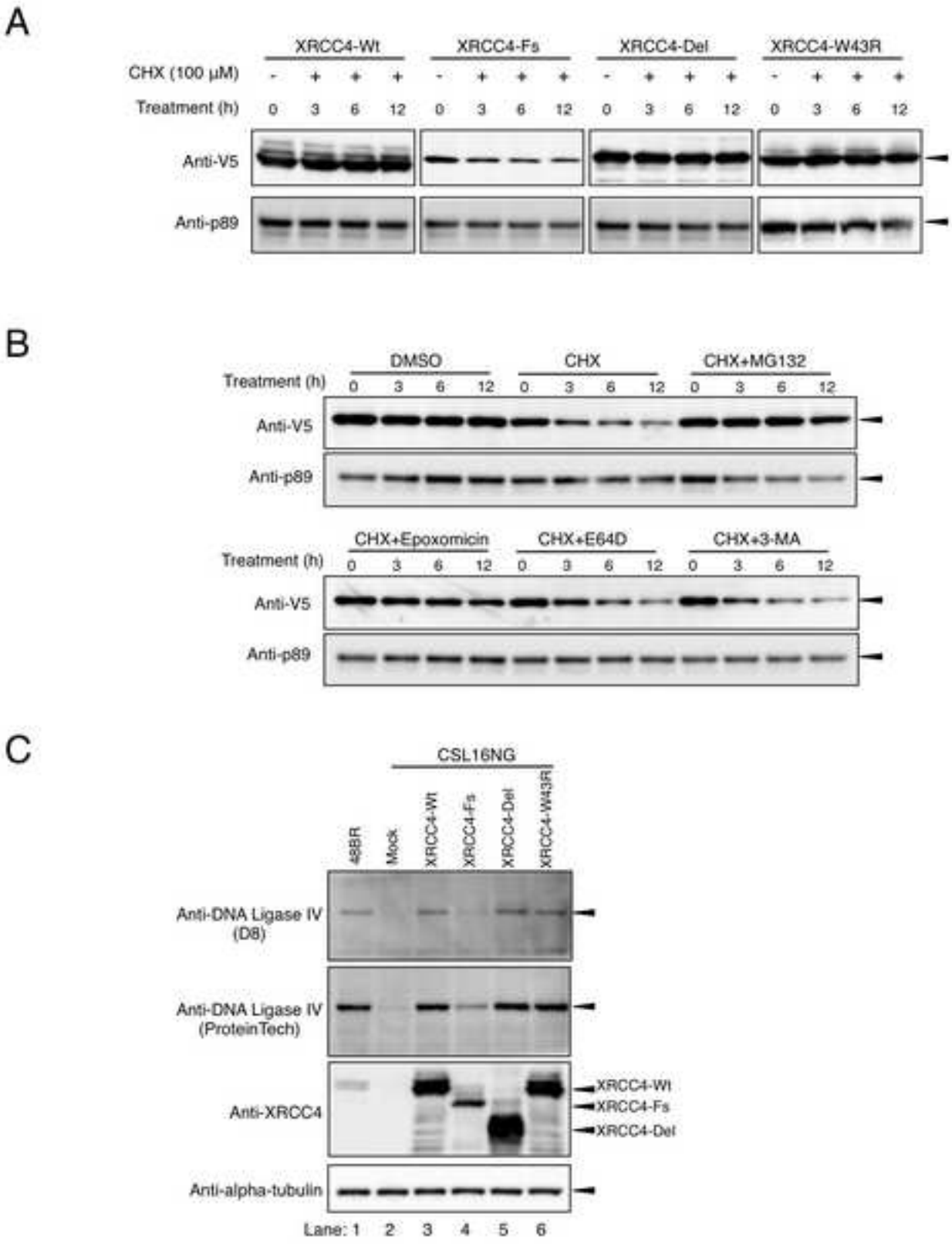

Figure 5

Click here to download high resolution image

Figure 5

A

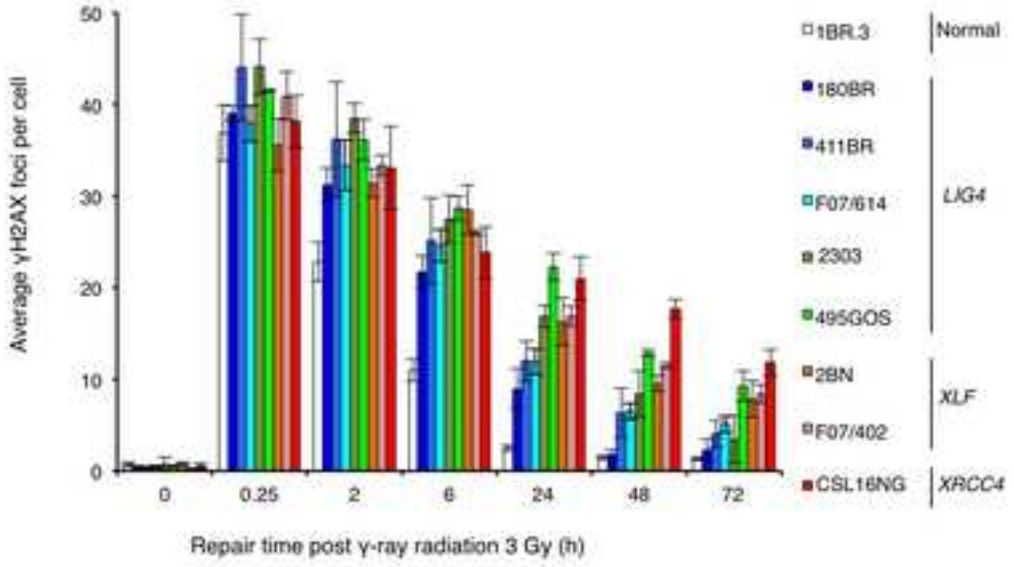

B

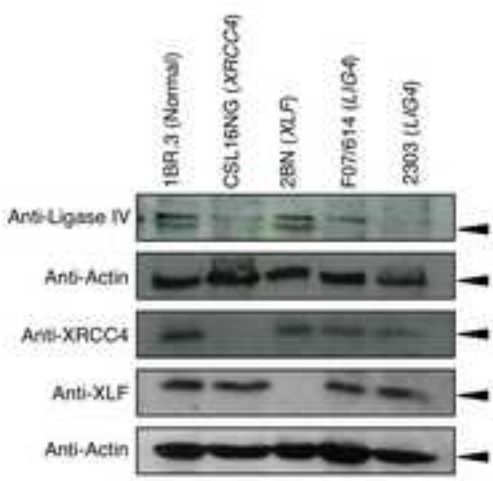

C

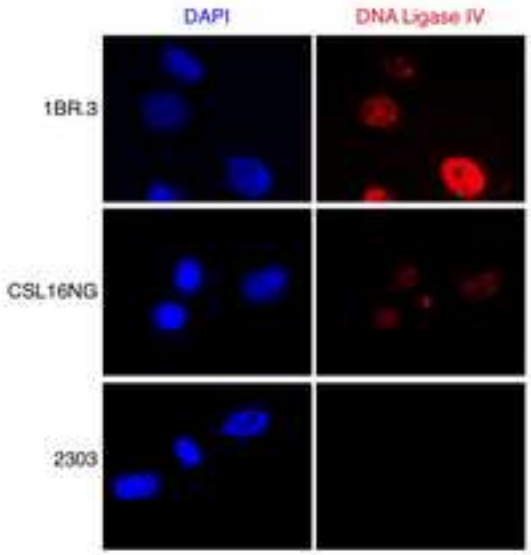

Supplementary Figure S1

Click here to download high resolution image

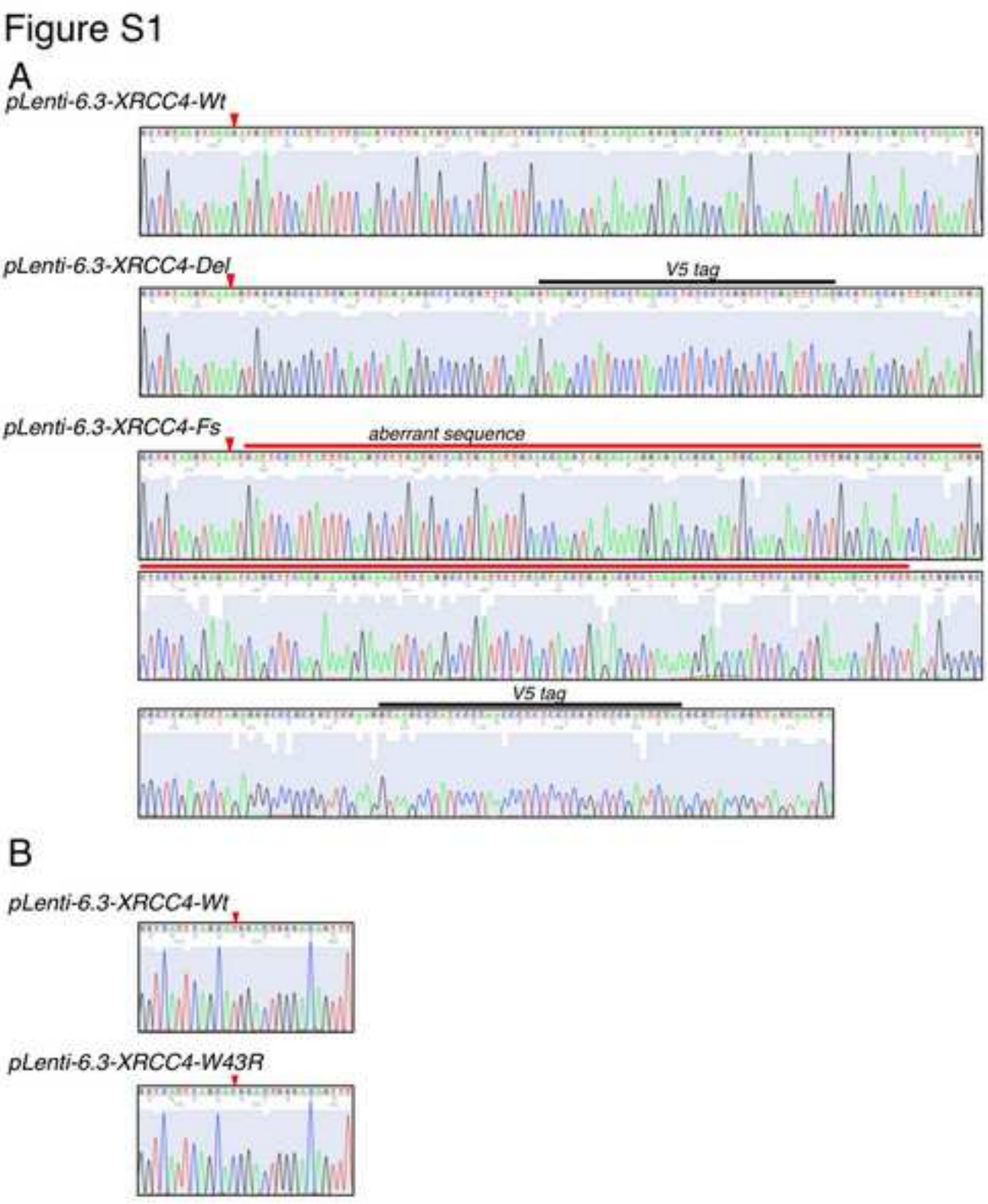

Supplementary Figure S2
Click here to download high resolution image

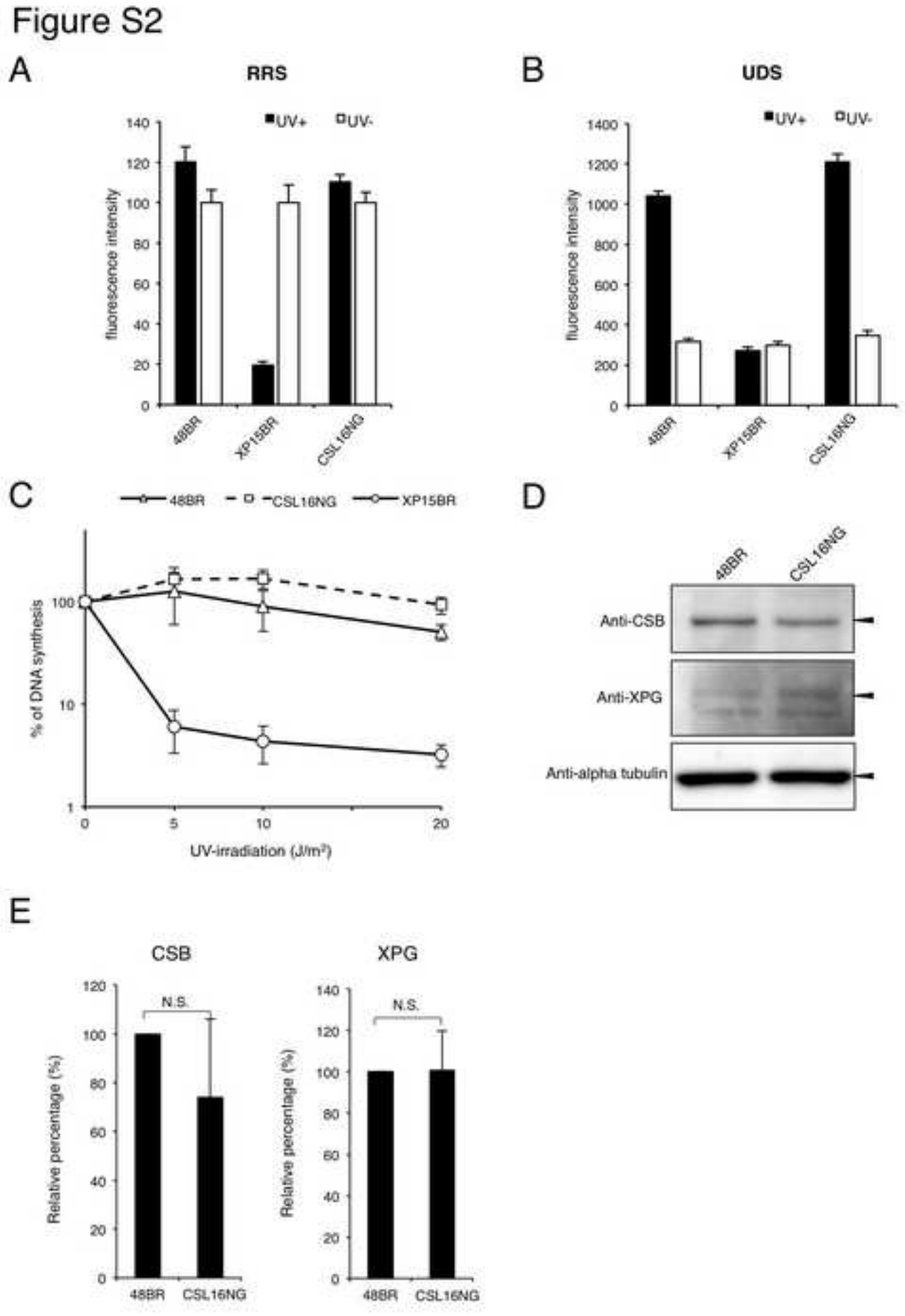

Supplementary Figure S3

Click here to download high resolution image

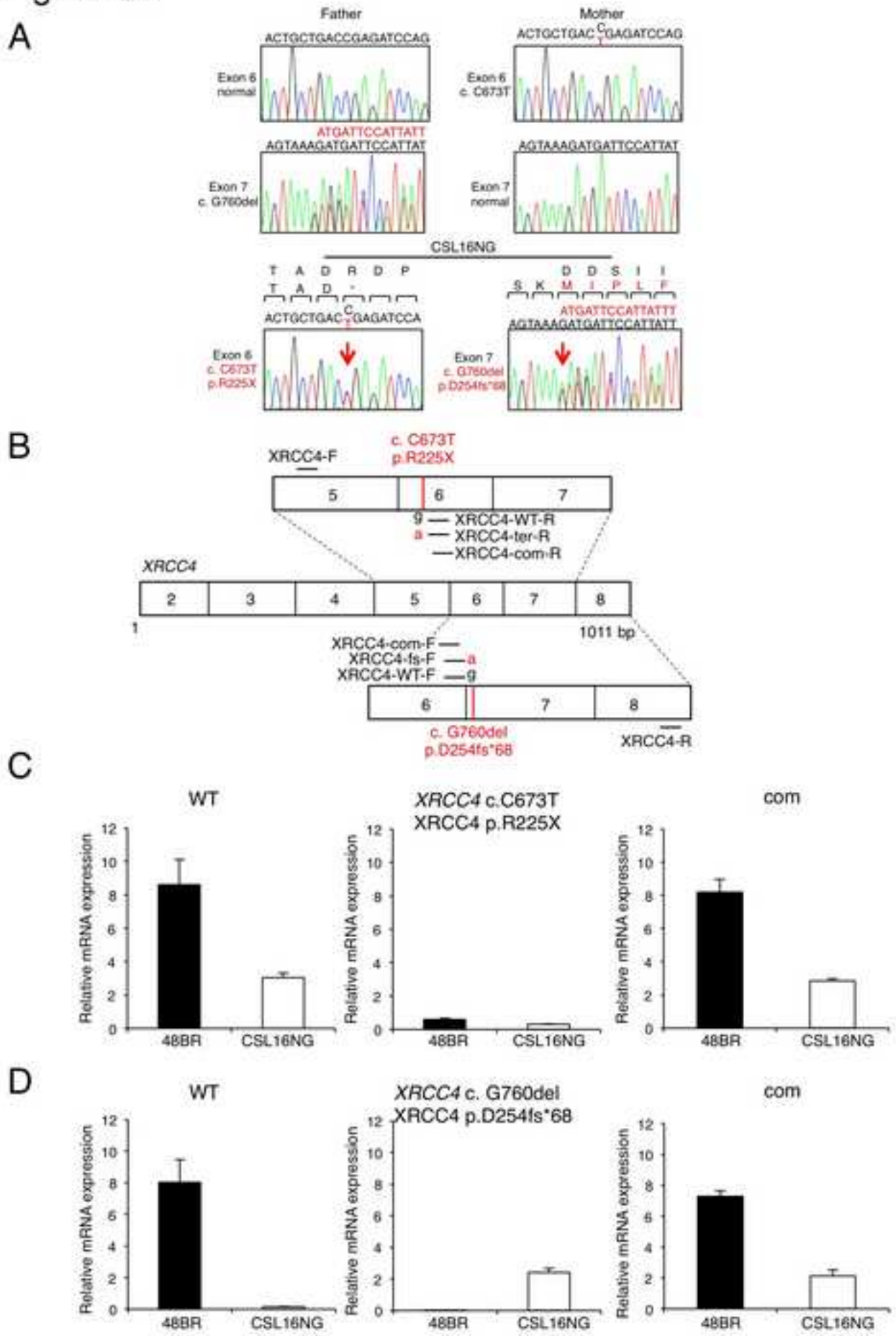

Supplementary Figure S4

Click here to download high resolution image

Figure S4

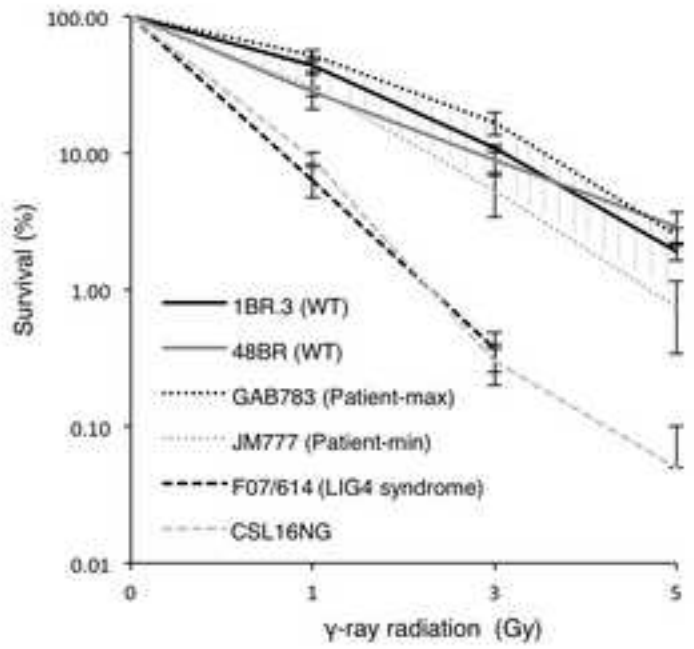

Supplementary Figure S5

Click here to download high resolution image

Figure S5

A

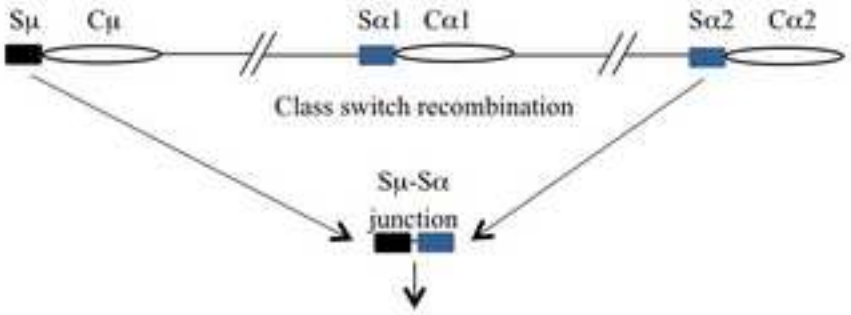

B

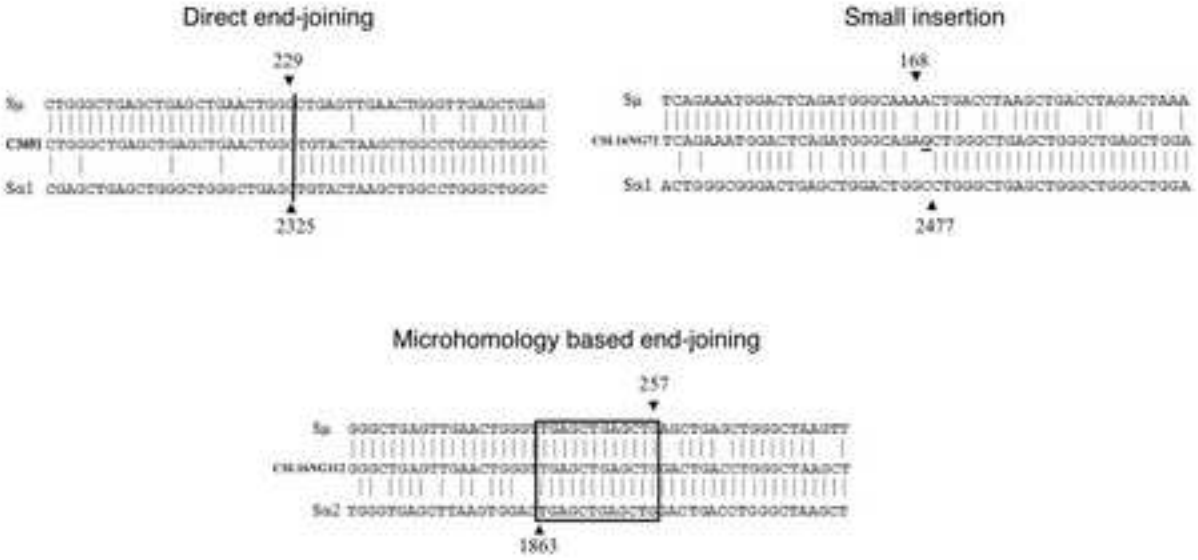

Supplementary Figure S6

Click here to download high resolution image

Figure S6

A

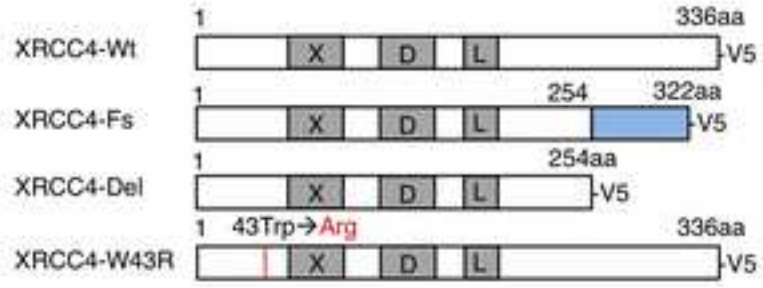

B

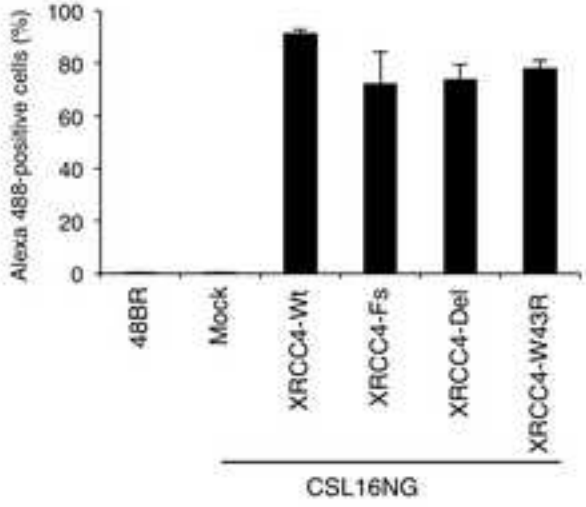

Supplementary Figure S7
Click here to download high resolution image

Figure S7

A

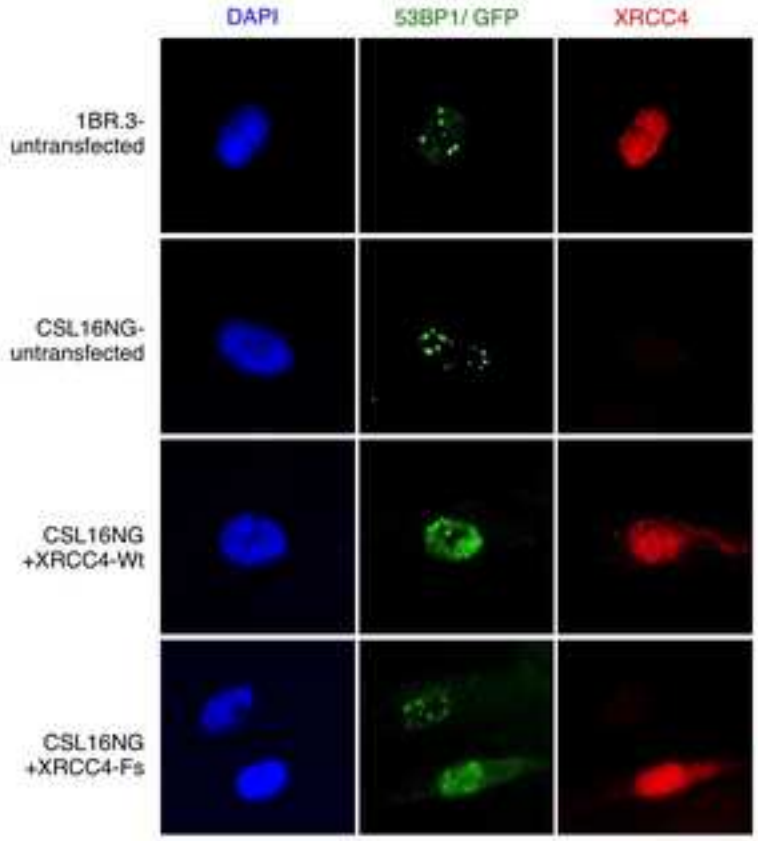

B

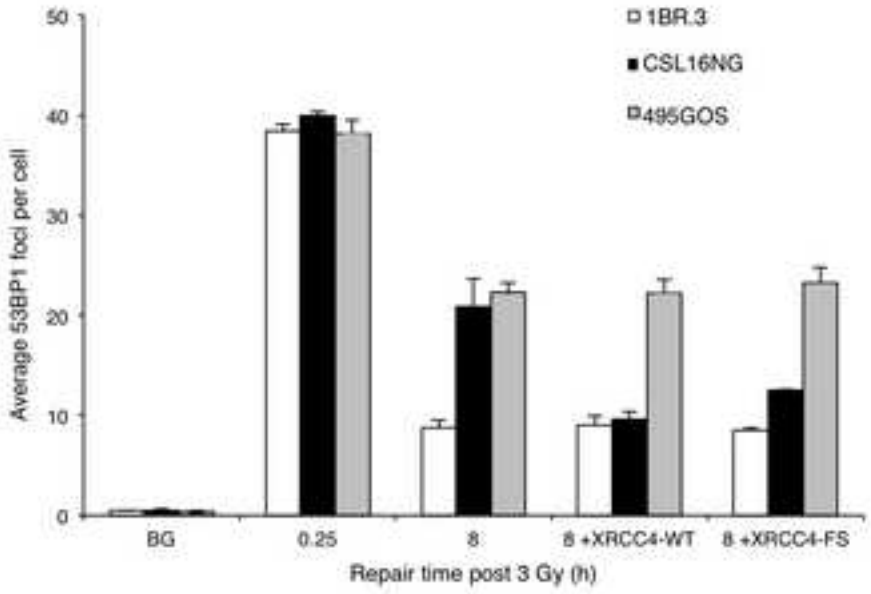

Supplementary Figure S8
Click here to download high resolution image

Figure S8

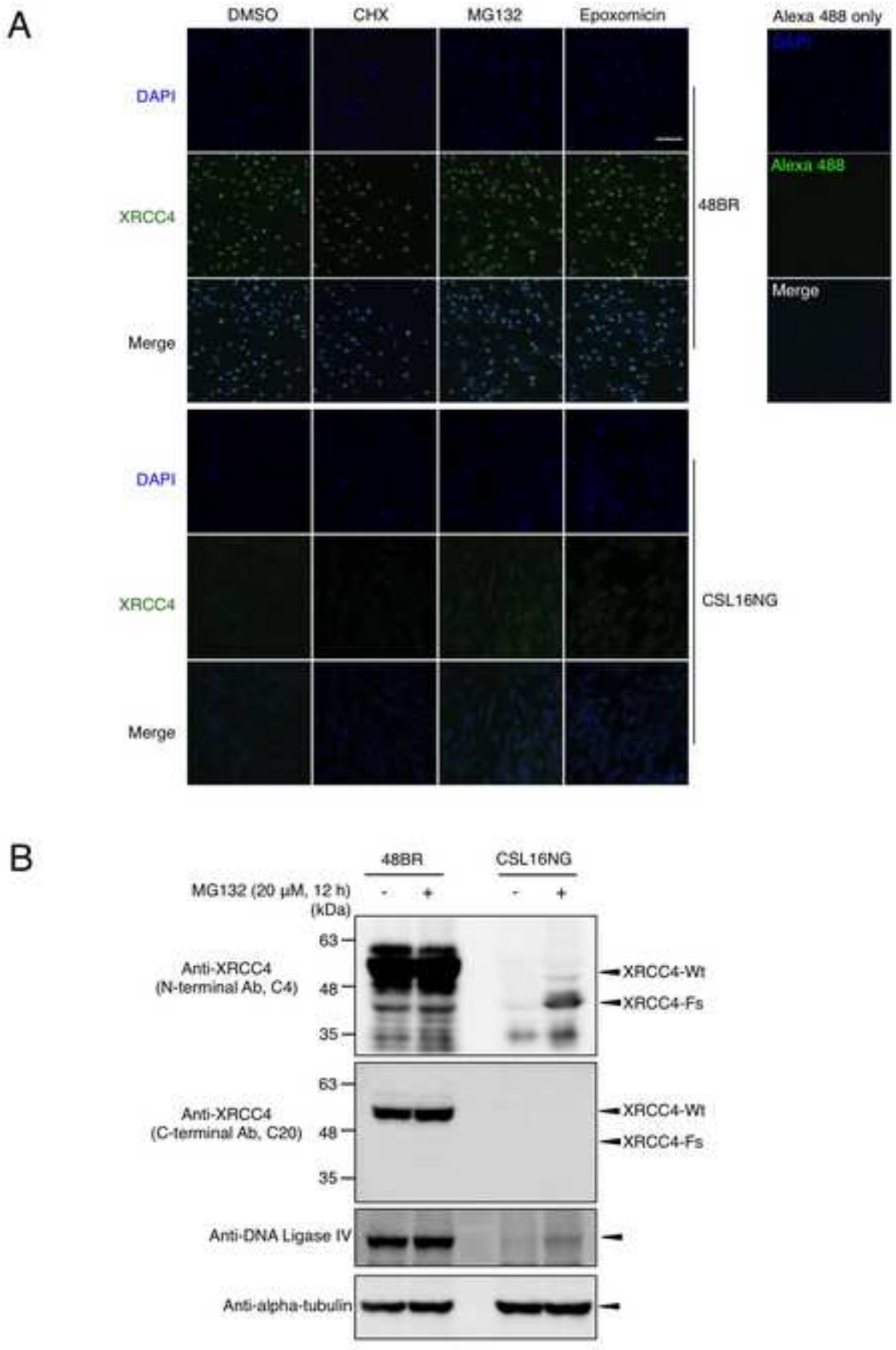

Supplementary Figure S9

Click here to download high resolution image